Supplementary Information

Rational Design of Covalent Cobaloxime-COF Hybrids for Enhanced Photocatalytic Hydrogen Evolution

Kerstin Gottschling,[†,‡,¶,§] Gökcen Savasci,[†,‡,¶,§] Hugo Vignolo-González,[†] Sandra Schmidt,[‡] Philipp Mauker,[‡,§] Tanmay Banerjee,[†] Petra Rovó,[‡,§] Christian Ochsenfeld,[‡,†,¶,§] and Bettina V. Lotsch[*,†,‡,¶,§]

†*Max Planck Institute for Solid State Research, Heisenbergstr. 1, 70569 Stuttgart, Germany*

‡*Department of Chemistry, University of Munich (LMU), Butenandtstr. 5-13, 81377 Munich, Germany*

¶*Cluster of Excellence e-conversion, Schellingstr. 4, 80799 Munich, Germany*

§*Center for Nanoscience (CeNS), Schellingstr. 4, 80799 Munich, Germany*

E-mail: b.lotsch@fkf.mpg.de

Table of Contents

List of Figures

List of Tables

Materials and methods

PXRD

PXRD patterns were recorded at room temperature on a Bruker D8 Discovery with Ni-filtered CuKα-radiation (1.5406 Å) and a position-sensitive detector (Lynxeye).

FT-IR

Fourier-transform infrared spectra were measured on a Jasco FT/IR-4100 or a Perkin Elmer Spectrum NX FT-IR System.

UV/Vis

UV/VIS samples were recorded in solid state on a Varian Cary 50.

Scanning electron microscopy

Scanning electron microscopy images were obtained with a Zeiss Merlin. A Tescan Vega 5130MM SEM, equipped with an Energy Dispersive Spectroscopy (EDS) detector X-MaxN (Oxford) was used for elemental mappings.

Structural models

Structural models were obtained with Materials Studio v6.0.0 Copyright © 2011 Accelrys Software using the Forcite Geometry optimization with Ewald electrostatic and van der Waals summation methods.

Sorption

Sorption measurements were performed on a Quantachrome Instruments Autosorb iQ MP with Argon at 87 K or with CO2 at 273, 288 or 298 K. Weight percentage was calculated by referencing to sorbent weight.

Solid-state NMR measurements

ssNMR was recorded on a Bruker Avance III-500 (500 MHz, 11.74 T) spectrometer. For ssNMR spectroscopy, the sample was filled in a 4 mm ZrO_2 rotor, which was mounted in a standard double resonance MAS probe (Bruker). NMR chemical shifts were referenced relative to TMS. The spinning rate was 12 kHz. A standard crosspolarization sequence with a 2.5 ms ramped contact pulse was used.

Fast MAS solid-state NMR measurements

Solid-state NMR experiments of [**1a**]-COF_{10} and [**Co-1a**]-COF_{10} were performed on a narrow-bore Bruker Neo spectrometer operating at 700 MHz ^{1}H Larmor frequency equipped with a 1.3 mm triple-resonance HCN MAS probe. In all experiments, unless otherwise stated, the spinning frequency was set to 55 555 Hz and the temperature was regulated so that the inner temperature was estimated to be 20 °C.In all experiments the $\pi/2$ pulse length was 1.55 μs for ^{1}H (161 kHz), 2.8 μs for ^{13}C (89 kHz). During direct or indirect ^{13}C evolution, an XiX decoupling was applied on the ^{1}H channel with a ^{1}H nutation frequency of 13.88 kHz. ^{1}H and ^{13}C chemical shifts were indirectly referenced to 4,4-dimethyl-4-silapentane-1-sulfonic acid (DSS). All spectra were acquired and processed using Bruker Topspin version 4.0, and later analyzed with Sparky.

1D experiments

For the spinning-frequency-dependent 1D ^{1}H experiments 128 scans were recorded over a spectral width of 100 kHz using a single pulse direct polarization experiment with a recycle delay of 1 s at spinning frequencies of 10, 20, 30, 40, 50, 55.55, and 58 kHz, as a reference, a static ^{1}H spectrum was also recorded with the same conditions. An inversion-recovery experiment was applied to determine the longitudinal relaxation time (T_1) of protons.

A direct polarization ^{13}C experiment was used for quantitative and qualitative signal intensity analysis. A total of 4096 (16384) scans were collected with a recycle delay of 25 s (1 s) for identifying the rigid (mobile) sites.

For the 1D ^{13}C-detected CP MAS experiments, a total of 1024 scans were collected over a spectral width of 71 kHz with a recycle delay of 1 s. During the CP the ^{1}H rf nutation frequency was tangentially ramped between 45 and 85 kHz, whereas the ^{13}C nutation frequency was kept constant at 10 kHz. The ^{13}C carrier was set to 130 ppm. A 13.88 kHz XiX ^{1}H decoupling was applied during the acquisition.

2D experiments

^{1}H-detected 2D ^{1}H-^{13}C correlation spectra were acquired using the double-quantum CP technique. The same CP steps were employed as for the 1D CP MAS experiment with a CP contact time of either 500 μs (short CP experiments) or 2250 μs (long CP experiments). The spectra were recorded with a spectral width of 20.8 kHz and 55.55 kHz in the ^{1}H and ^{13}C dimensions, respectively using 356 indirect time points, 128 scans and 0.5 s recycle delay time for [**1a**]-COF_{10} and 240 indirect time points, 704 scans and 0.7 s recycle delay time for [**Co-1a**]-COF_{10}. The carrier for ^{1}H and ^{13}C was centered at 6 and 130 ppm, respectively.

2D ^{1}H-^{1}H homonuclear through-space double quantum - single quantum correlation spectra were measured with $R14_4^{-2}$ symmetry sequence, with a $R = 180_0$ symmetry element using the same number of elements both excitation and reconversion of the DQCs, and a t_1 dwell time of 36 μs corresponding to a rotor-synchronized F1 spectral width. 96 complex t_1 points

were acquired with 64 scans for each indirect time points. A four step phase cycle was used to obtain the double-quantum coherence in the t_1 dimension. A States method was used for signal acquisition.

Quantum-Chemical Calculations

Atom positions and lattices of all periodic structures were optimized on RI-PBE-D3/def2-TZVP[1–4] level of theory using an acceleration scheme based on the resolution of the identity (RI) technique and the continuous fast multipole method (CFMM)[5–7] implemented[8,9] in Turbomole version V7.1.[10] The CFMM uses multipole moments of maximum order 20, together with a well-separateness value of 3 and a basis function extent threshold of 10E-9 a.u. Grid 7 was used for the numerical integration of the exchange-correlation term. The norm of the gradient was converged to 10E-4 a.u. and the total energy to 10E-8 Hartree within the structure optimization using the gamma point approximation.

Parameters for molecular dynamics simulations for COF pores were prepared using antechamber.[11] Force field minimizations and dynamics were performed using the NAMD program package[12,13] using GAFF parameters.[14] Periodic boundary conditions and particle mesh Ewald summation (PME) with a cutoff value of 12 Å were employed. The modeled COF pore was minimized using the conjugate gradient algorithm in 1000 steps by constraining the coordinates for the COF backbone excluding all hydrogen atoms that were allowed to relax along with the functionalized linker of the **1a** linker moiety. The system was then heated to 300 K in 30 ps and equilibrated subsequently for 15 ns with time steps of 2 fs employing the SETTLE algorithm.

NMR chemical shifts were obtained on B97-2/pcSseg-1[15,16] level of theory using the FermiONs++[17,18] program package performed on cut models of previously obtained structures.

Synthetic procedures

1,3,5-triformylbenzene and 3-(azidomethyl)pyridine were used as purchased. 2,5-diethoxyterephthalohydrazide was synthesized according to known procedures as follows. All reactions were performed under Ar atmosphere with dry solvents and magnetically stirred, unless otherwise noted.

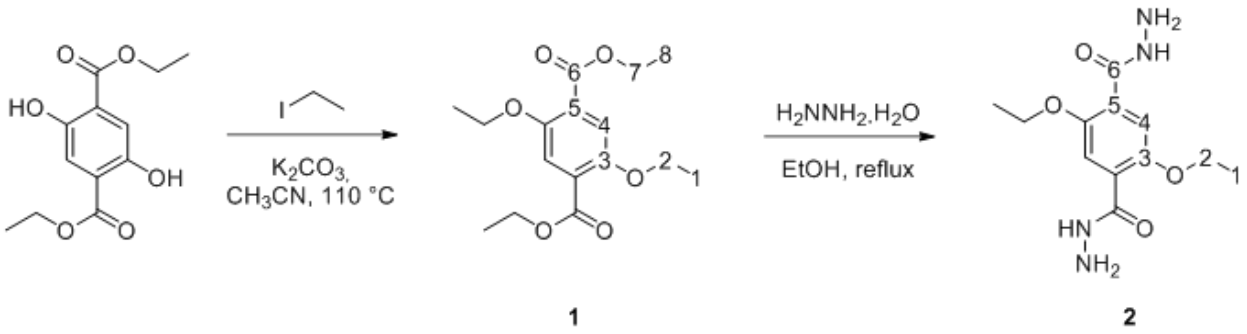

Diethyl-2,5-diethoxyterephthalate (1)

Diethyl-2,5-dihydroxyterephthalate (4 mmol, 1.05 g, 1 eq) and potassium carbonate (13.2 mmol, 1.82 g, 3.3 eq) were suspended in acetonitrile (10 mL). Iodoethane (13.2 mmol, 1.07 mL, 3.3 eq) was added. After the reaction mixture was refluxed for 72 h, the solvent was removed. The brownish residue was added into water and extracted with ethyl acetate. The organic extract was dried over magnesium sulfate. The solvent was removed to give the product as a light yellow solid (1.20 g, 3.87 mmol, 97%).

^{1}H-NMR (400 MHz, $CDCl_3$): δ = 7.34 (s, 2H, H_{arom}), 4.37 (q, J = 7.1 Hz, 4H, Me-CH_2), 4.08 (q, J = 7.0 Hz, 4H, O-C-H_2-CH_3), 1.41 (dt, J = 15.2, 7.0 Hz, 12H, CO-CH_2-CH_3/ COO-CH_2-CH_3) ppm.

^{13}C-NMR (101 MHz, $CDCl_3$): δ = 166.1 (C6), 151.8 (C3), 125.1 (C5), 117.1 (C4), 65.8 (C2), 61.41 (C7), 14.94 (C1), 14.39 (C8) ppm.

HR-ESI-MS: calc. for $C_{16}H_{22}O_6$: $[M]^+$: 310.1416; found: 310.1408.

2,5-Diethoxyterephthalohydrazide (2)

Diethyl 2,5-diethoxy)terephthalate (3.96 mmol, 1.2 g, 1 eq) was suspended in a solution of ethanol/toluene (20 mL, 1:1). Hydrazine hydrate (39.6 mmol, 1.94 mL, 10 eq) was added. The reaction mixture was heated to 110 °C for 8 h. The solvent was evaporated to yield an off-white solid (903 mg, 3.20 mmol, 81%).

^{1}H-NMR (400 MHz, DMSO-d_6): δ = 9.24 (s, 2H, N-H), 7.38 (s, 2H, H_{arom}), 4.58 (s, 4H, O-C-H_2-CH_3), 4.12 (q, J = 6.9 Hz, 4H, N-H_2), 1.35 (t, J = 6.9 Hz, 6H, -CH_3) ppm.

^{13}C-NMR (101 MHz, DMSO-d_6): δ = 163.8 (C6), 149.53 (C3), 125.0 (C5), 114.7 (C4), 64.81 (C2), 14.54 (C1) ppm.

HR-EI-MS: calc. for $C_{16}H_{29}N_6O_4$ $[M]^+$: 282.1328; found: 282.1433.

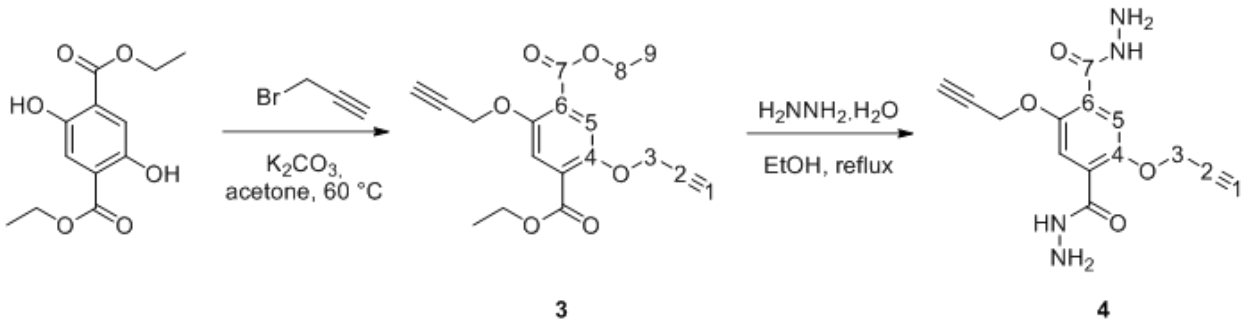

Diethyl 2,5-bis(prop-2-yn-1-yloxy)terephthalate (3)

Diethyl 2,5-dihydroxyterephthalate (1.05 g, 4.00 mmol, 1.00 eq) and potassium carbonate (2.21 g, 16.0 mmol, 4.00 eq) were flushed with argon and dissolved in acetone (20 mL). The mixture was degased (3x argon/3x vacuum) and propargyl bromide (2.38 g, 16.0 mmol, 4.00 eq) was added. The reaction mixture was stirred at 60 °C for 72 h. The reaction was monitored by TLC (CH_2Cl_2:MeOH 9:1) and after complete conversion, the reaction mixture was added on ice. The solid was filtered, washed with water and dried *in vacuo* for 48 h, yielding the product (1.24 g, 3.75 mmol, 94%) as a light brown solid. ^{1}H-NMR (400 MHz,

$CDCl_3$): δ = 7.56 (s, 2H-$_{arom}$), 4.76 (d, J = 2.4 Hz, 4H, Me-CH_2), 4.39 (q, J = 7.1 Hz, 4H, O-CH_2-CH_2), 2.54 (t, J = 2.4 Hz, 2H, -CCH), 1.40 (t, J = 7.1 Hz, 6H, -CH_3) ppm.

^{13}C-NMR (101 MHz, $CDCl_3$): δ = 165.2 (C7), 151.4 (C4), 126.0 (C6), 119.0 (C5), 78.17 (C2), 76.36 (C1), 61.68 (C8), 58.38 (C3), 14.37 (C9) ppm.

HR-ESI-MS: calc. for $C_{18}H_{18}O_6$ $[M]^+$: 330.1103; found: 330.1096.

2,5-Bis(prop-2-yn-1-yloxy)terephthalohydrazide (4)

A suspension of diethyl 2,5-bis(prop-2-yn-1-yloxy)terephthalate (**3**) (0.90 g, 2.9 mmol, 1.0 eq) in EtOH/toluene (1:1, 15 mL) was degased (3x argon/3x vacuum). Hydrazine hydrate (1.49 mL, 1.53 g, 30.3 mmol, 10.0 eq) was added and the solution was stirred at 80 °C over night. The resulting white precipitate was filtered and washed with EtOH and CH_2Cl_2, yielding the product (0.70 mg, 2.3 mmol, 79%) as a white solid.

^{1}H-NMR (400 MHz, DMSO-d_6): δ = 9.30 (s, 2H, N-H), 7.48 (s, 2H, H_{arom}), 4.89 (d, J = 2.4 Hz, 4H, O-C-H_2-CH_3), 4.57 (s, 4H, N-H2) 3.62 (t, J = 2.4 Hz, 2H, -CCH) ppm.

^{13}C-NMR (101 MHz, DMSO-d_6): δ = 163.5 (C7), 148.8 (C4), 125.6 (C6), 115.4 (C5), 78.97 (C2), 78.85 (C1), 56.78 (C3) ppm.

HR-ESI-MS: calc. for $C_{14}H_4N_4O_4$ $[M]^+$: 302.1015; found: 302.1014.

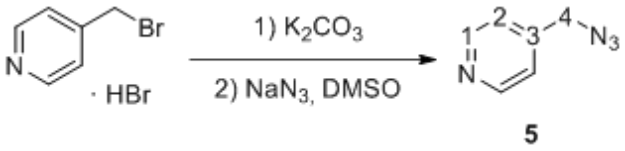

5

4-(azidomethyl)pyridine (5)

4-(Bromomethyl)pyridine hydrobromide (1.26 g, 5.00 mmol, 1.00 eq) was dissolved in DMF (15 mL). Potassium carbonate (0.96 g, 5.00 mmol, 1.00 eq) was added and the reaction

mixture was stirred at room temperature for 15 min. Sodium azide (0.49 g, 7.50 mmol, 1.50 eq) was added and the reaction mixture was stirred at room temperature for 72 h. EtOAc (10 mL) and water (10 mL) were added, the organic layer was separated and the reaction mixture was extracted with EtOAc (3x 20 mL). The combined organic layers were washed with water (3x 25 mL), dried over $MgSO_4$ and the solvent was removed *in vacuo* yielding 5 (0.33 g, 2.46 mmol, 49%) as a light yellow oil.

^{1}H-NMR (400 MHz, $CDCl_3$): δ = 8.63 (d, J = 6.1 Hz, 2H, 1-H), 7.27 (d, J = 6.0 Hz, 2H, 2-H), 4.43 (s, 2H, 4-H) ppm.

^{13}C-NMR (101 MHz, $CDCl_3$): δ = 150.24 (C1), 144.71 (C3), 122.53 (C2), 53.42 (C4) ppm.

HR-EI-MS: calc. for $C_6H_6N_4$ $[M]^+$: 134.0593 found: 134.0585.

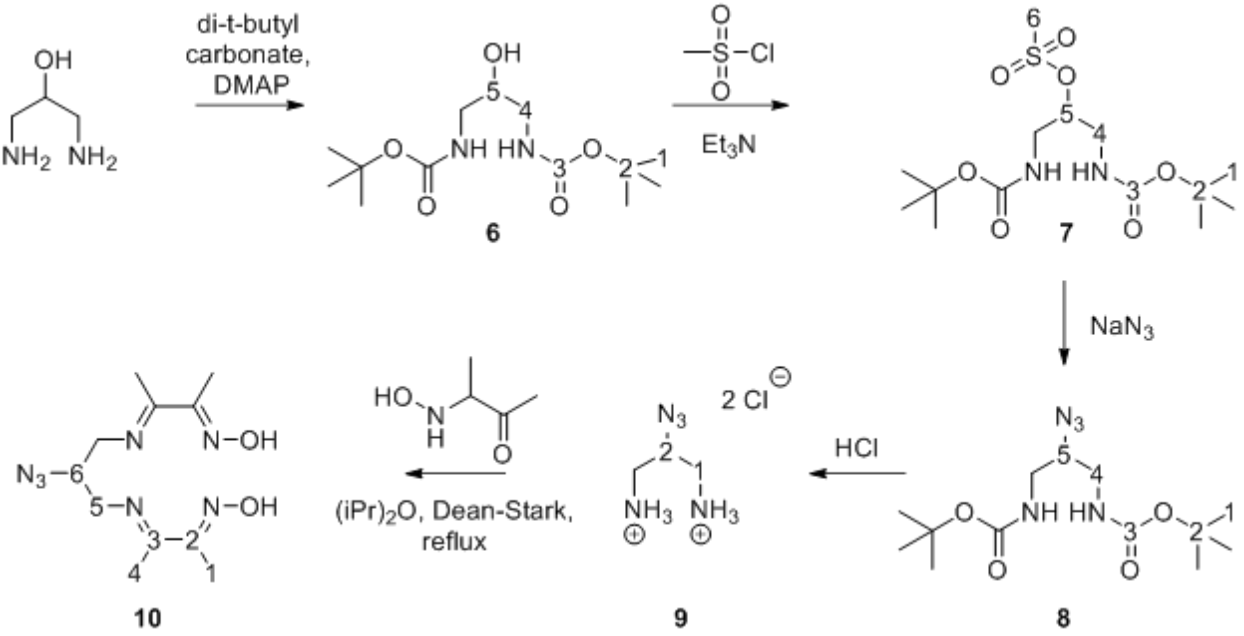

Di-*tert*-butyl (2-hydroxypropane-1,3-diyl)dicarbamate (6)

1,3-Diamino-2-propanol (4.6 g, 51 mmol, 1.00 eq) was dissolved in water (50 mL). A solution of di-*tert*-butylpyrocarbonat (23 g, 105 mmol, 2.05 eq) in acetonitrile (50 mL) was added at 0 °C. DMAP (13 g, 107 mmol, 2.1 eq) was added at 0 °C. The reaction mixture was stirred

at 0 °C for 2 h and for further 16 h at room temperature as the ice bath melted. The crude product was extracted with dichloromethane (200 mL) and 1M HCl. The combined organic layers were washed with saturated $NaHCO_3$ solution (3x 50 mL) and brine (2x 25 mL). The organic layer was dried over $MgSO_4$ and the solvents were removed in vacuo, yielding 6 (19 g, 48 mmol, 95%) as a white solid.

^{1}H-NMR (400 MHz, $CDCl_3$): δ = 6.99 (s, 2H, NH), 5.05 (s, 1H, OH), 3.73 (q, J = 5.5, 5.1 Hz, 1H, 4-H), 3.34 – 3.09 (m, 4H, 3-H), 1.44 (s, 18H, 1-H) ppm.

^{13}C-NMR (101 MHz, $CDCl_3$): δ = 162.54 (C3), 79.63 (C2), 70.49 (C5), 40.92 (C4), 28.30 (C1) ppm.

LR-EI-MS: calc. for $C_{13}H_{27}N_2O_5$ $[M+H]^+$: 291.18 found: 291.24.

2-[(*tert*-Butoxycarbonyl)amino]-1-[[(*tert*-butoxycarbonyl)amino]-methyl]ethyl methanesulfonate (7)

Di-*tert*-butyl (2-hydroxypropane-1,3-diyl)dicarbamate (6) (8.0 g, 20 mmol, 1.0 eq) and triethylamine (4.8 mL, 3.5 g, 34 mmol, 1.7 eq) were dissolved in dry CH_2Cl_2. Methanesulfonyl chloride (3.1 mL, 4.6 g, 40 mmol, 2.0 eq) was added dropwise at 0 °C while stirring under argon. The reaction mixture was allowed to warm to room temperature and was stirred for 18 h. Water was slowly added to quench the reaction. The organic layer was separated, washed with water and dried over $MgSO_4$. The solvents were removed *in vacuo* and the crude product was recrystallized with hexanes, yielding 7 (7.3 g, 20 mmol, 98%) as a white solid.

^{1}H-NMR (400 MHz, $CDCl_3$): δ = 5.14 (s, 2H, NH), 4.70 – 4.62 (m, 1H, 5-H), 3.55 – 3.24 (m, 4H, 4-H), 3.09 (s, 3H, 6-H), 1.44 (s, 18H, 1-H) ppm.

^{13}C-NMR (101 MHz, $CDCl_3$): δ = 157.46 (C3), 80.02 (C2), 71.50 (C5), 43.79 (C4), 41.83 (C6), 28.51 (C1) ppm.

HR-EI-MS: calc. for $C_{14}H_{29}N_2O_7S$ $[M+H]^+$: 369.1617 found: 369.1692.

Di-*tert*-butyl (2-azidopropane-1,3-diyl)dicarbamate (8)

2-[(*tert*-Butoxycarbonyl)amino]-1-[[(*tert*-butoxycarbonyl)amino]methyl]ethyl methanesulfonate (7) (0.50 mg, 1.4 mmol, 1.0 eq) was dissolved in dry DMF (5 mL). A suspension of sodium azide (0.35 mmol, 5.4 mmol, 4.0 eq) in dry DMF (2.5 mL) was added and the reaction mixture was stirred at 80 °C for 18 h. Water (25 mL) and CH_2Cl2 (25 mL) were added, the organic layer was separated, washed with water (3x 25 mL) and dried over mgSO4. The solvents were removed in vacuo, yielding 8 (0.33 g, 1.0 mmol, 71%) as a light yellow solid.

^{1}H-NMR (400 MHz, $CDCl_3$): δ = 5.17 (s, 2H, NH), 3.73 – 3.49 (m, 1H, 5-H), 3.36 – 3.05 (m, 4H, 4-H), 1.41 (s, 18H, 1-H) ppm.

^{13}C-NMR (101 MHz, $CDCl_3$): δ = 162.58 (C3), 79.75 (C2), 60.99 (C5), 40.94 (C4), 28.37 (C1) ppm.

HR-EI-MS: calc. for $C_{13}H_{26}N_5O_4$ $[M+H]^+$: 316.19065 found: 316.1960.

2-Azidopropane-1,3-diamine dihydrochloride (9)

Di-*tert*-butyl (2-azidopropane-1,3-diyl)dicarbamate (8) (0.90 g, 2.8 mmol, 1.0 eq) was dissolved in EtOAc (3 mL). Hydrochloric acid (6 M, 1.5 mL, 8.9 mmol, 8.0 eq.) was added. The reaction mixture was stirred for 8 h and relaxed over night at 5 °C. The obtained crystals were filtered and washed with EtOAc, yielding 9 (0.32 g, 1.7 mmol, 60%) as white crystals.

^{1}H-NMR (400 MHz, DMSO-d_6): δ = 8.51 (s, 6H, NH3+), 4.28 (tt, J = 8.5, 4.1 Hz, 1H, 2-H), 3.16 (dd, J = 13.4, 4.1 Hz, 2H, 1-H), 2.91 (dd, J = 13.4, 8.8 Hz, 2H, 1-H) ppm.

^{13}C-NMR (101 MHz, DMSO-d_6): δ = 57.03 (C2), 40.19 (C1) ppm.

2-Butanone, 3,3'-[(2-azido-1,3-propanediyl)dinitrilo]bis-2,2'-dioxime (10)

A solution of 2-azidopropane-1,3-diamine dihydrochloride (9) (0.20 g, 1.1 mmol, 1.0 eq), 2,3-butanedione monoxime (0.21 g, 2.1 mmol, 2.0 eq) and sodium hydrogen carbonate (0.18 g, 2.1 mmol, 2.0 eq) in a two-phase mixture of water and iPr2O (1:4, 25 mL) was refluxed for 18 h using a DEAN-STARK apparatus. The reaction mixture was hot-filtered, washed with CH_2Cl_2 and the solvent removed in vacuo. The residue was recrystallized in heptane and the solvent was evaporated, yielding 10 (0.25 g, 0.87 mmol, 82%) as a white solid.

^{1}H-NMR (400 MHz, DMSO-d_6): δ = 11.43 (s, 2H, OH), 3.67 – 3.57 (m, 1H, 6-H), 3.41 – 3.19 (m, 4H, 5-H), 1.99 (s, 6H, 1-H/4-H), 1.92 (s, 6H, 1-H/4-H) ppm.

^{13}C-NMR (101 MHz, DMSO-d_6): δ = 153.01 (C3), 149.94 (C2), 59.73 (C6), 52.08 (C5), 20.74 (C4), 9.31 (C1) ppm.

HR-EI-MS: calc. for $C_{11}H_{20}N_7O_2$ $[M+H]^+$: 282.16002 found: 282.16726.

COF synthesis

All products were obtained as fluffy solids. To remove residual starting materials, powders were washed intensely with DMF, THF and dichloromethane and subsequently dried in a vacuum desiccator overnight.

COF-42

To a Biotage© 2 mL microwave vial, 1,3,5 triformylbenzene (0.066 mmol, 10.7 mg, 2 eq) and 2,5-diethoxyterephthalohydrazide (0.099 mmol, 27.9 mg, 3 eq) were added. Dioxan (0.25 mL), mesitylene (0.75 mL) and acetic acid (6M, 150 µL) were added. The vial was sealed and heated under microwave irradiation at 160 °C for 30 min. Subsequently, the vial was heated in a muffle furnace at 120 °C for 72 h. After cooling to room temperature, the

solid was filtered and washed with DMF (3 x 2 mL), THF (3 x 2 mL) and DCM (3 x 2 mL) to yield a light-yellow powder.

$\mathbf{pCOF}_{10}$

For the copolymerized systems, corresponding amounts of 2,5-diethoxyterephthalohydrazide were replaced by 2,5-bis(2-(dimethylamino)ethoxy)terephthalohydrazide while the procedure was retained as described before. Solvents were used according to Table S1. The products yielded as yellow to orange powders.

Postmodification

Route (I)

1st step:

1 eq 1a/1b/2, 0.5 equ $CoCl_2 \cdot 6\ H_2O$ and 1.1 eq dimethylglyoxime (in the case of **1a** and **1b**) was dissolved in hot ethanol. Upon oxidation with air for 1 h, the dispersion turns brown and yields [**Co-1a**]/[**Co-1b**]/[**Co-2**] after filtration and washing with water, ethanol, ethyl acetate and acetone.

2nd step:

1 eq $pCOF_{10}$, 2 eq [**Co-1a**]/[**Co-1b**]/[**Co-2**], 0.25 eq $CuSO_4 \cdot 5\ H_2O$ and 0.5 eq sodium ascorbate were dispersed in a 1:1 mixture of degassed toluene and *tert*-butyl alcohol under argon. Stirring for 72 h at room temperature yields [**Co-1a**]/[**Co-1b**]/[**Co-2**]-COF_{10} after filtration and washing with water, ethanol, ethyl acetate and acetone.

For controlling the cobaloxime content of the resulting samples, experimental conditions were altered as follows: Temperature: rt, 40 °C, 60 °C. Reaction time: 72 h, 120 h, 7 days, 14 days Concentration: 1 eq = 0.0111 mmol in 8 mL solvent, 1 eq = 0.0111 mmol in 4 mL solvent, 1 eq = 0.0222 mmol in 8 mL solvent

Route (II)

1st step:

1 eq $pCOF_{10}$, 2 eq 1a/1b/2, 0.25 eq $CuSO_4 \cdot 5\ H_2O$ and 0.5 eq sodium ascorbate were despersed in a 1:1 mixture of degassed toluene and *tert*-butyl alcohol under argon. Stirring at room temperature yields [**1a**]/[**1b**]/[**2**]-COF_{10} after filtration and washing with water, ethanol, ethyl acetate and acetone.

For controlling the cobaloxime content of the resulting samples, experimental conditions were altered as follows: Temperature: rt, 40 °C, 60 °C. Reaction time: 72 h, 120 h, 7 days, 14 days Concentration: 1 eq = 0.0111 mmol in 8 mL solvent, 1 eq = 0.0111 mmol in 4 mL solvent, 1 eq = 0.0222 mmol in 8 mL solvent

2nd step:

1 eq [**1a**]/[**1b**]/[**2**-COF_{10}, 0.5 eq $CoCl_2 \cdot 6\ H_2O$ and 1.1 eq dimethylglyoxime (in the case of **1a** and **1b**) were dispersed in ethanol. Upon oxidation with air for 1h, the dispersion turns brown and yields [**Co-1a**]/[**Co-1b**]/[**Co-2**]-COF_{10} after filtration and washing with water, ethanol, ethyl acetate and acetone.

Photocatalysis measurements

In a typical photocatalysis experiment, 5 mg of COF hybrid were suspended in 10 mL of acetonitrile and water in a ratio of 4:1 at pH 8 containing 100 µL triethanolamine (TEOA) as sacrificial donor. Irradiation with 100 mW cm^{-1} AM1.5 radiation resulted in hydrogen evolution.

Spectral distribution of our solar simulator was nominally AM 1.5G based on a housed

Xe lamp and a AM 1.5G filter, which is presented below, while the beam integrated power intensity had a recorded value of 45 mW cm^{-2}. During experiments, intensity was adjusted to 100 mW cm^{-2} but at a more uncertain spectral distribution which was not recorded in this document. For some experiments measured a few months later, the Xe lamp of our solar simulator was replaced achieving a more stable spectral distribution with an integrated beam power of 100 mW cm^{-2}, which is also shown. As different lamps were used for different measurements, photocatalytic activity of the samples were compared in photonic efficiencies in the main text.[19]

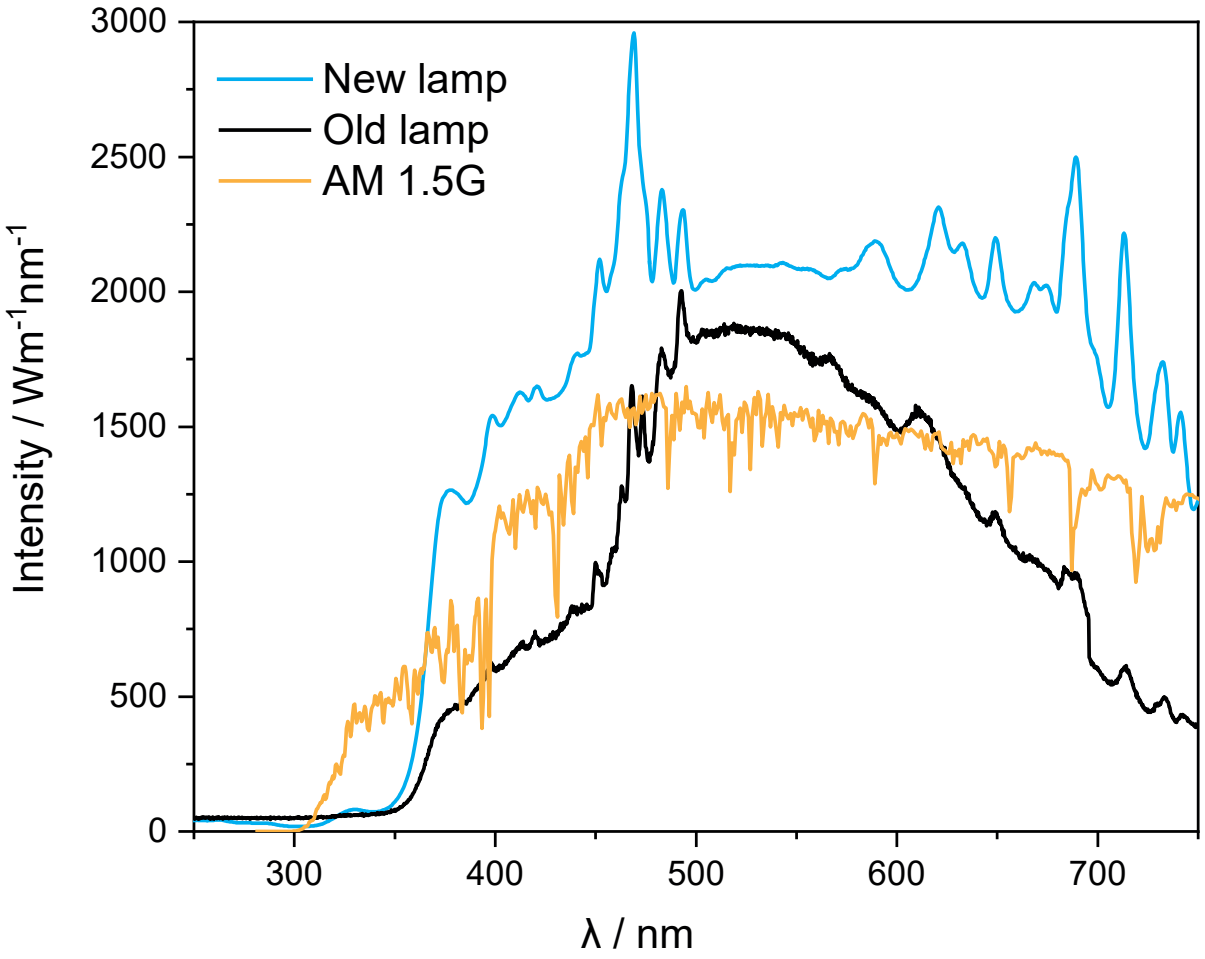

Figure S1: Light intensities of the solar simulator that was used earlier for the measurements in the main manuscript (old lamp, black), the lamp that was used for the experiments in ESI where stated (new lamp, blue), compared to AM 1.5G (yellow).

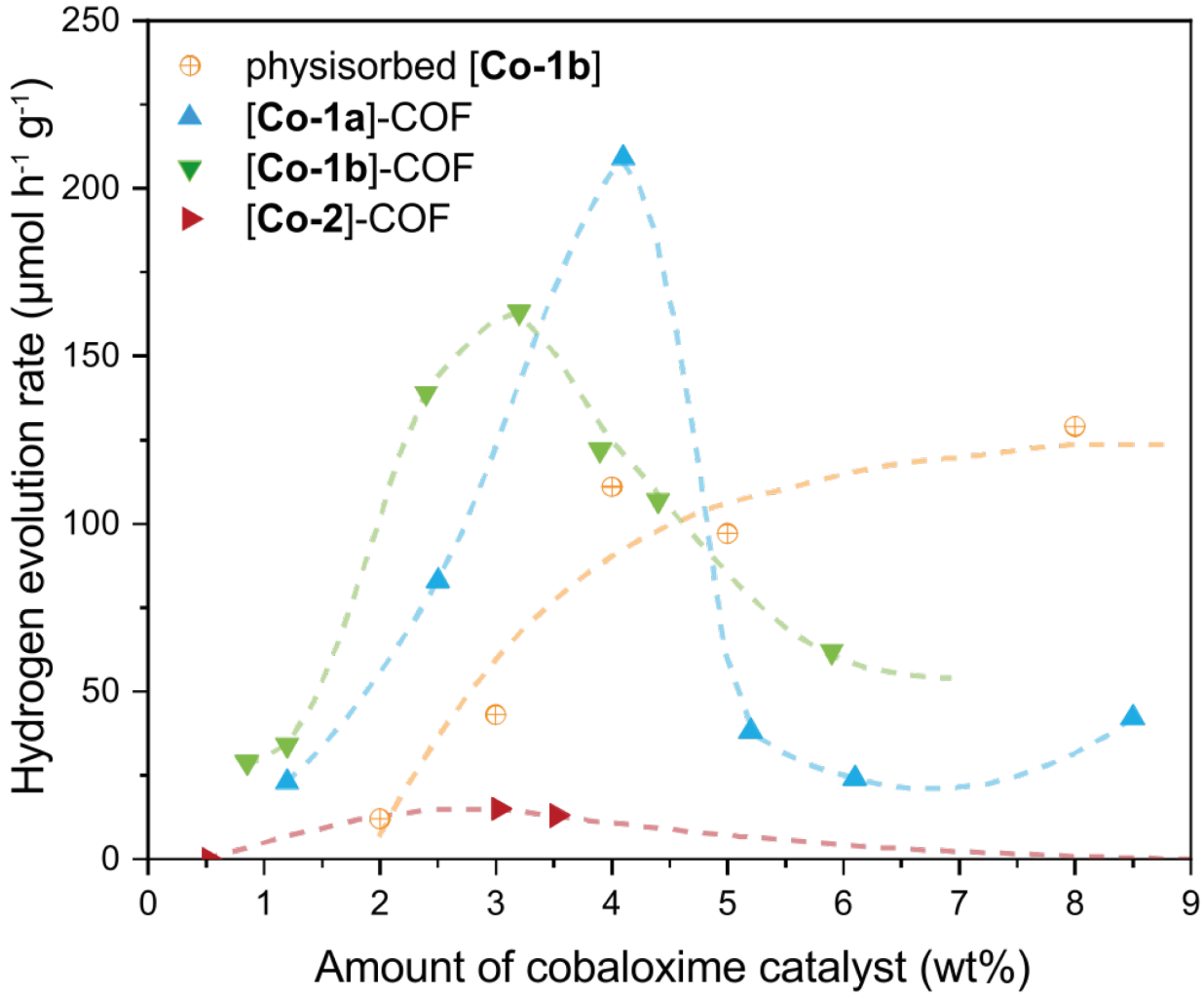

Figure S2: Comparison of hydrogen evolution rates for hybrid samples and COF-42 with physisorbed [**Co-1b**] measured with the old lamp.

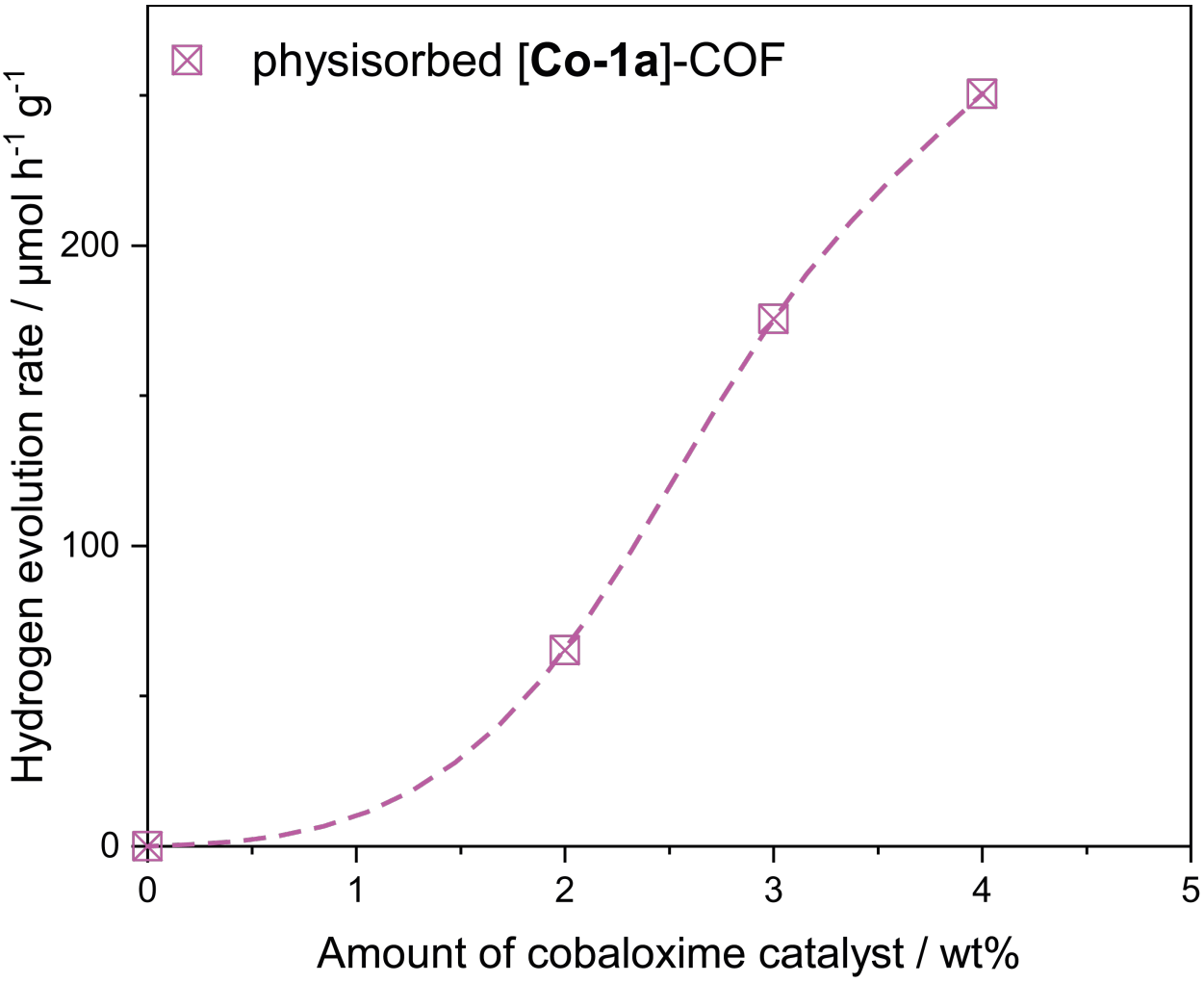

Figure S3: Hydrogen evolution rate for [**Co-1a**]-COF measured with the new lamp.

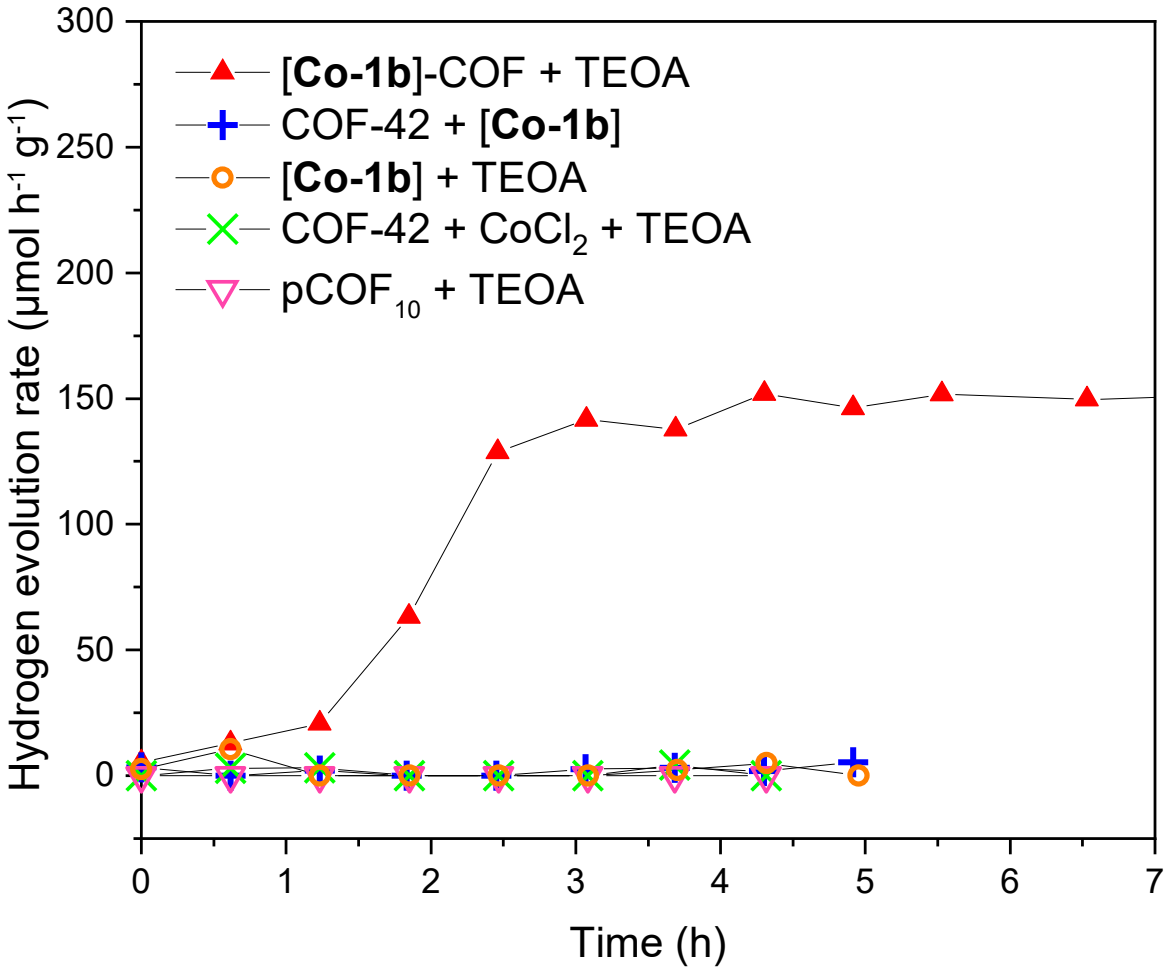

Figure S4: Photocatalytic hydrogen evolution experiments in acetonitrile and water in a ratio of 4:1 at pH 8. Red triangles: [**Co-1b**]-COF with TEOA as sacrificial donor. Blue pluses: COF-42 with [**Co-1b**], no sacrificial donor added. Orange circles: [**Co-1b**] with TEOA as sacrificial donor, no COF added. Green crosses: COF-42 with TEOA as sacrificial donor and $CoCl_2$. Pink triangles: $pCOF_{10}$ with TEOA as sacrificial donor.

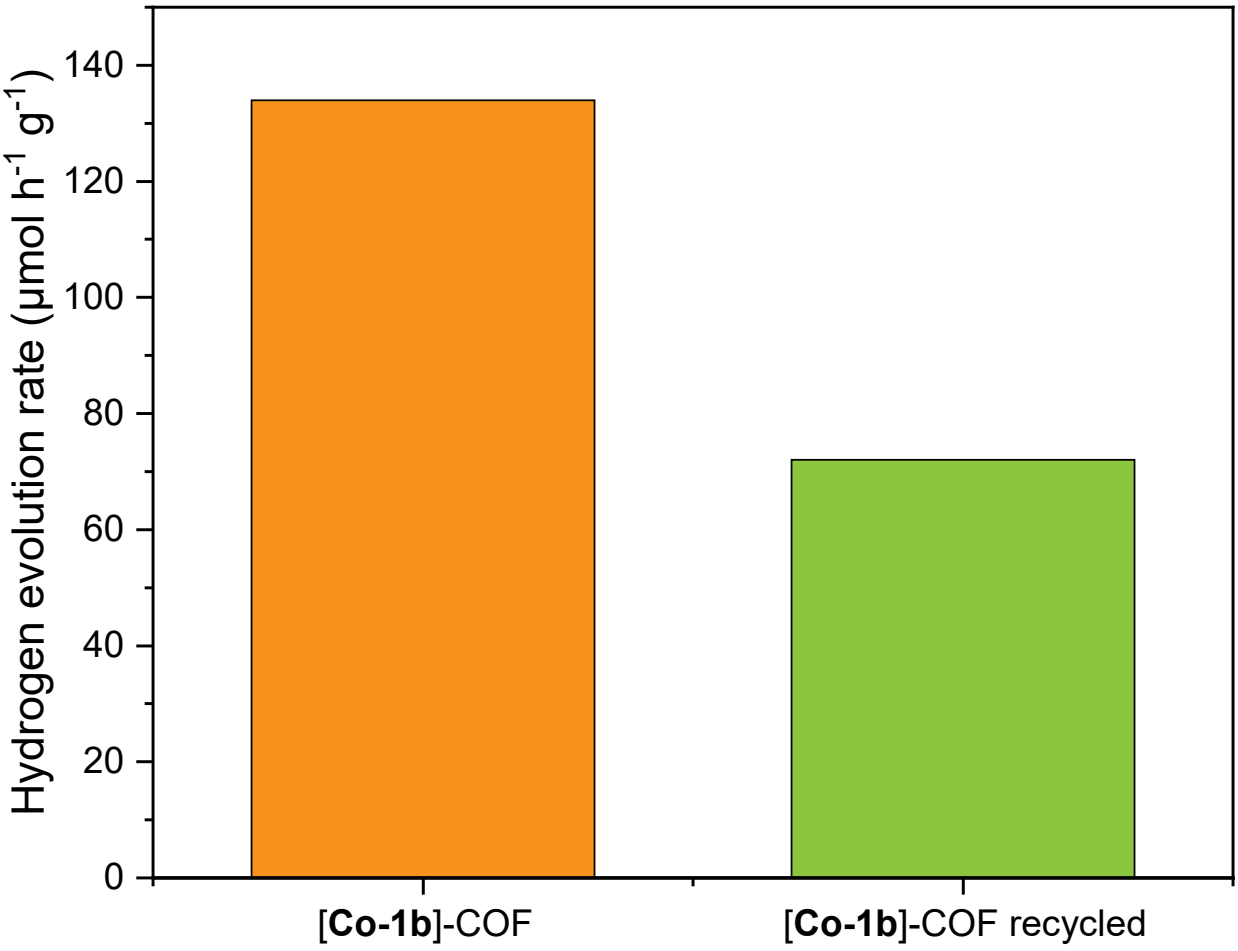

Figure S5: Photocatalytic activity of [**Co-1b**]-COF with 4.2 wt% cobaloxime content. Orange: first measurement, green: Measurement after recycling.

Sorption analysis

Table S1: BET surface areas based on argon sorption measurements of the presented COFs.

Sample name	BET surface area (m^2 g^{-1})
$pCOF_{10}$	1839
[**1a**]-COF	1306
[**1b**]-COF	1117
[**2**]-COF	1031
[**Co-1a**]-COF	900
[**Co-1b**]-COF	1330
[**Co-2**]-COF	1101

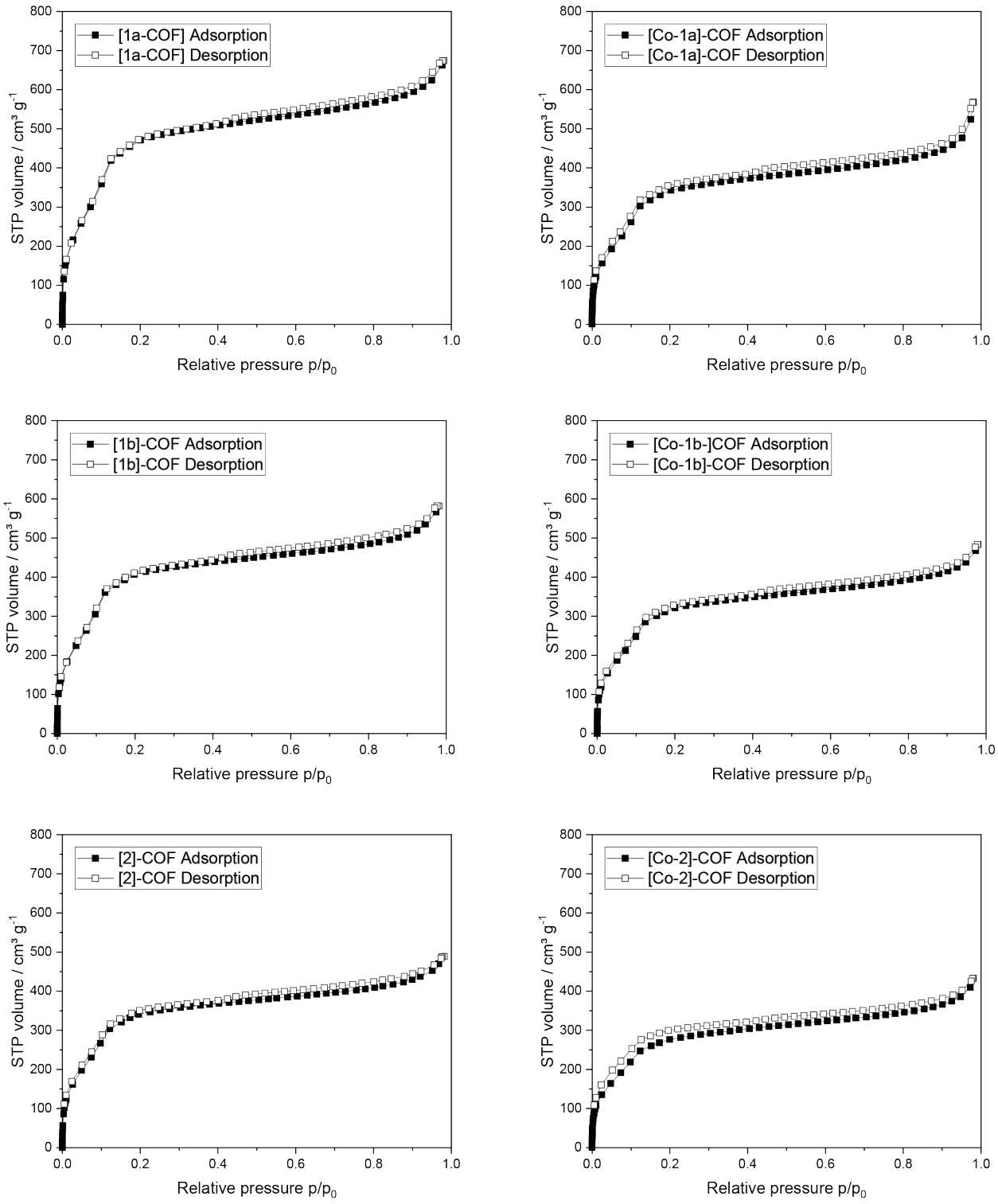

Figure S6: Argon isotherms of **1a**-COF, **1b**-COF, **2**-COF, [**Co-1a**]-COF, [**Co-1b**], and [**Co-2**]-COF

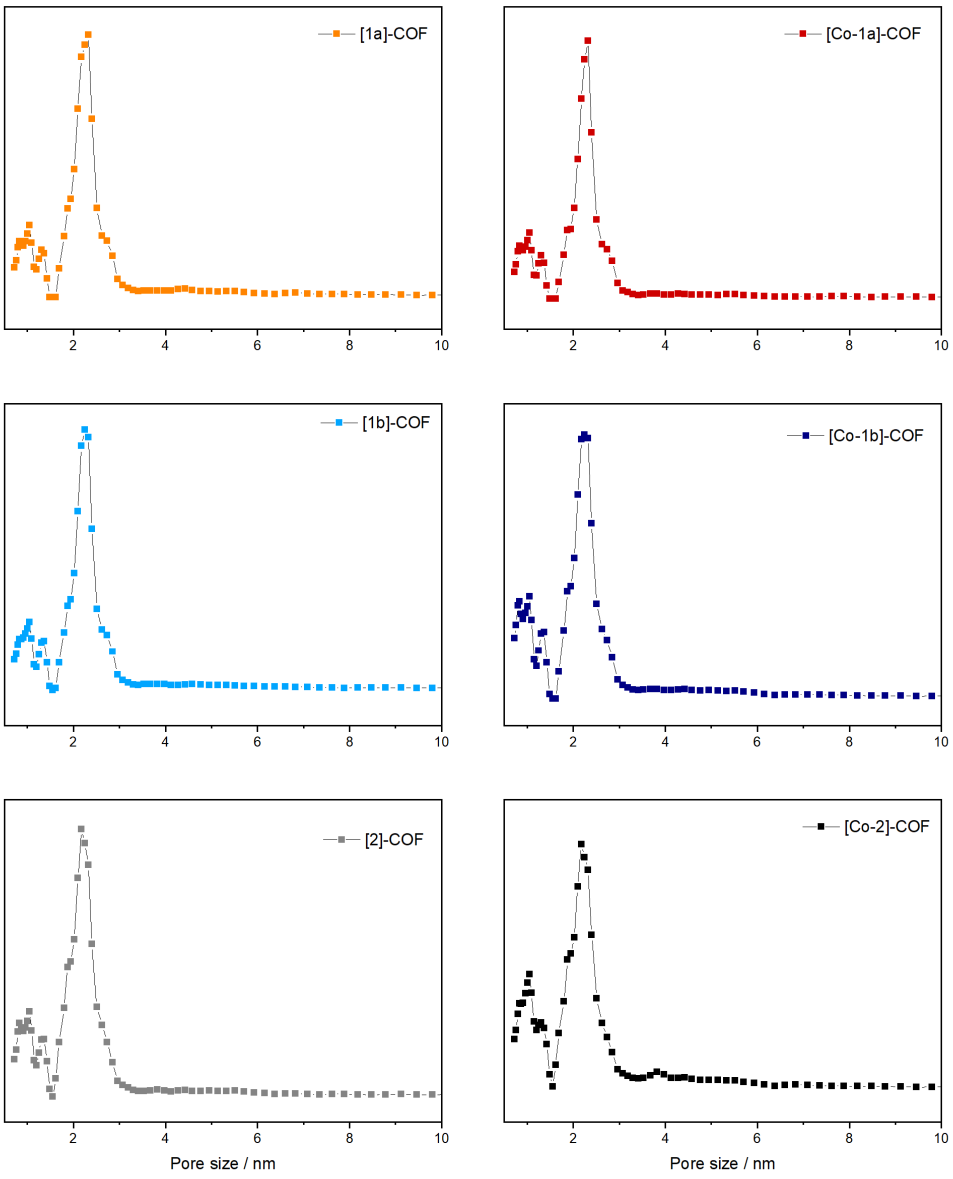

Figure S7: Pore size distributions of **1a**-COF, **1b**, **2**-COF][**Co-1a**]-COF, [**Co-1b**], and [**Co-2**]-COF.

Powder X-ray diffraction

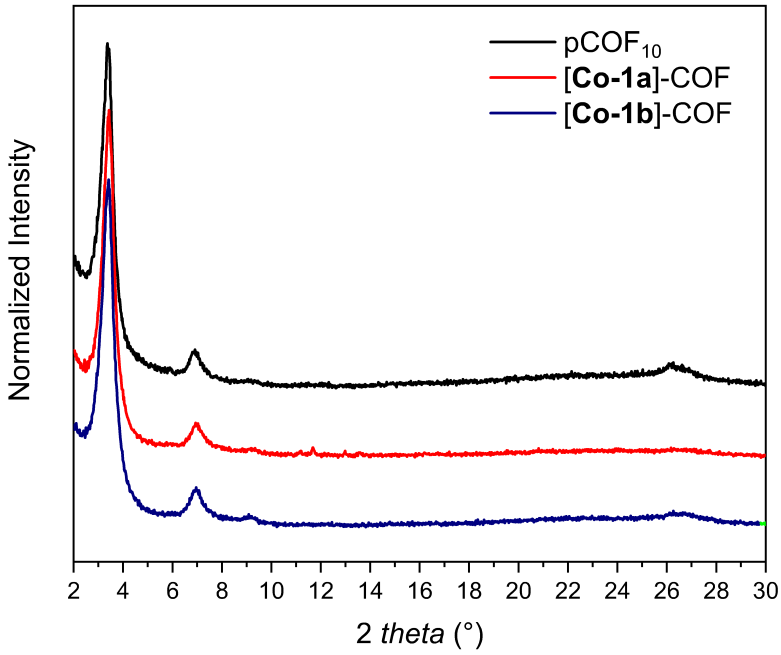

Figure S8: Powder X-ray diffractogramms of $pCOF_{10}$, [**Co-1a**]-COF and [**Co-1b**]-COF.

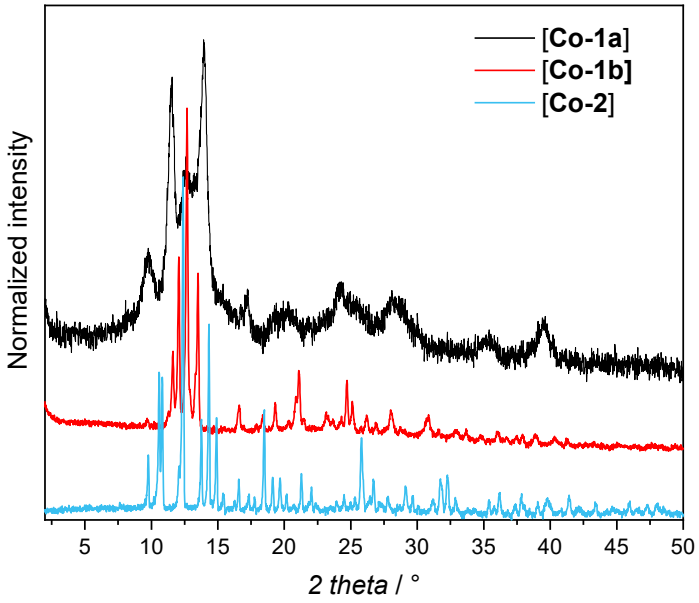

Figure S9: Powder X-ray diffractogramms of [**Co-1a**], [**Co-1b**], and [**Co-2**].

Scanning electron microscopy

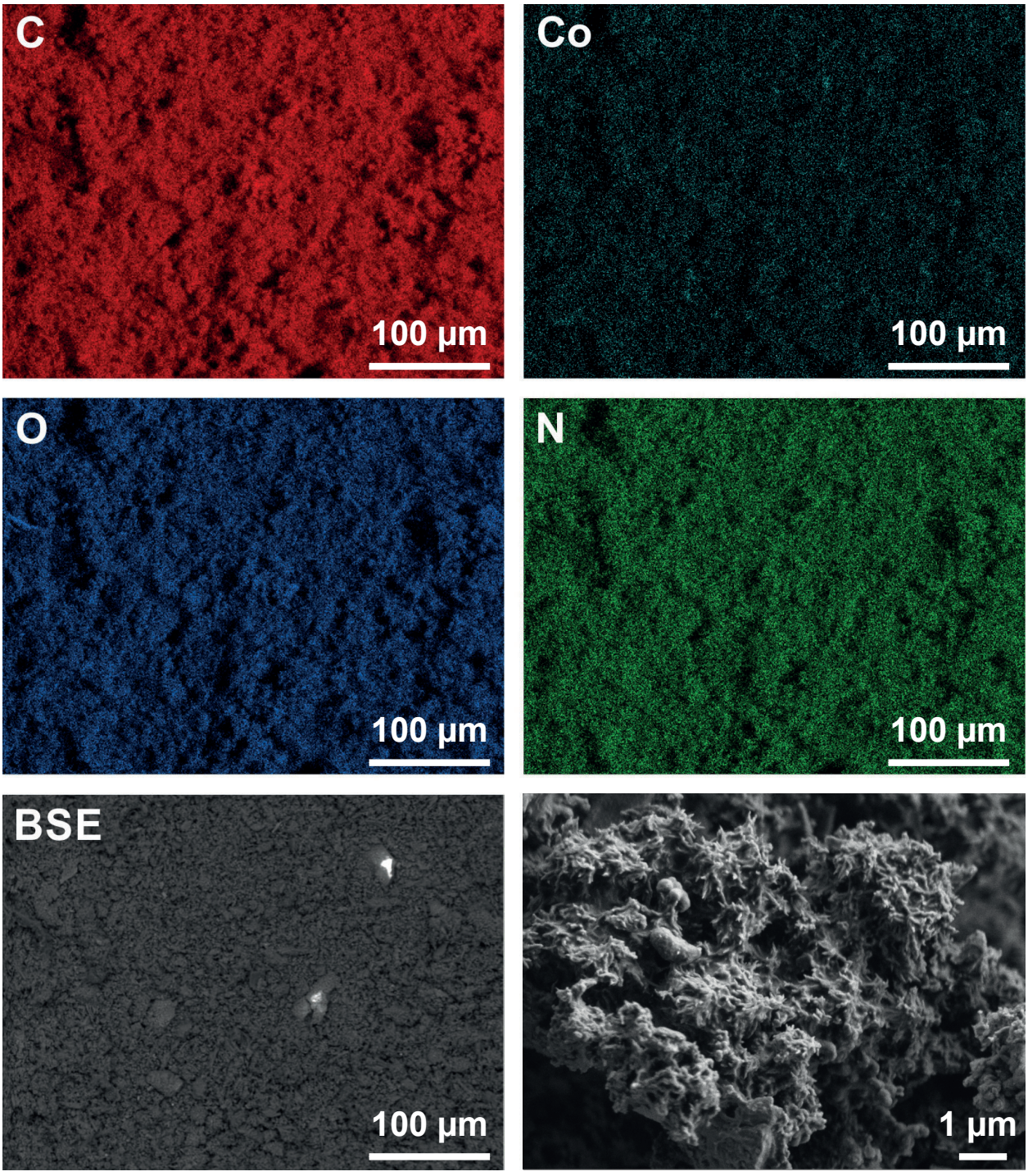

Figure S10: Scanning electron microscopy image of [**Co-1a**]-COF.

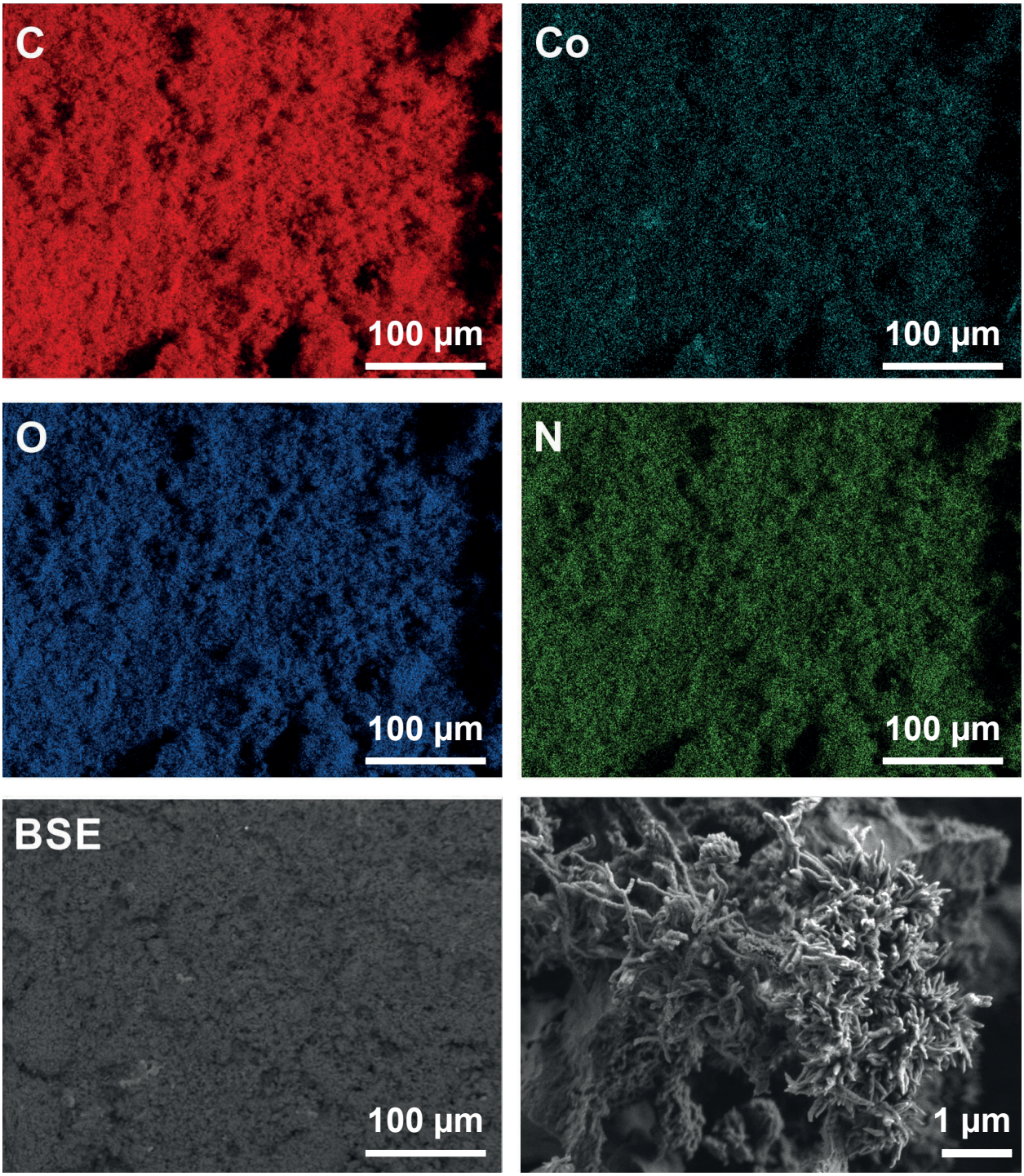

Figure S11: Scanning electron microscopy image of [**Co-1b**]-COF.

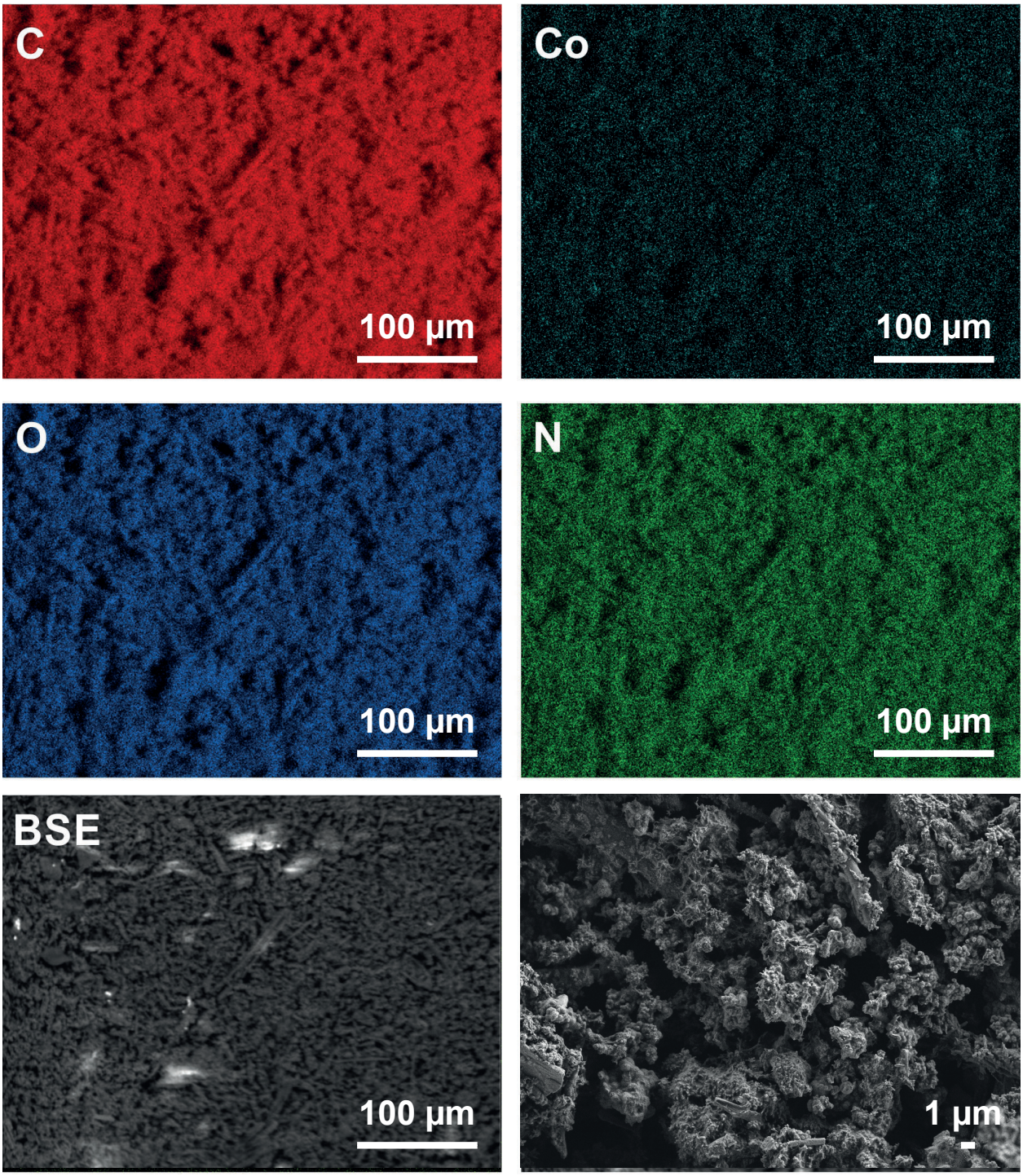

Figure S12: Scanning electron microscopy image of [**Co-2**]-COF.

Photoluminescence spectroscopy

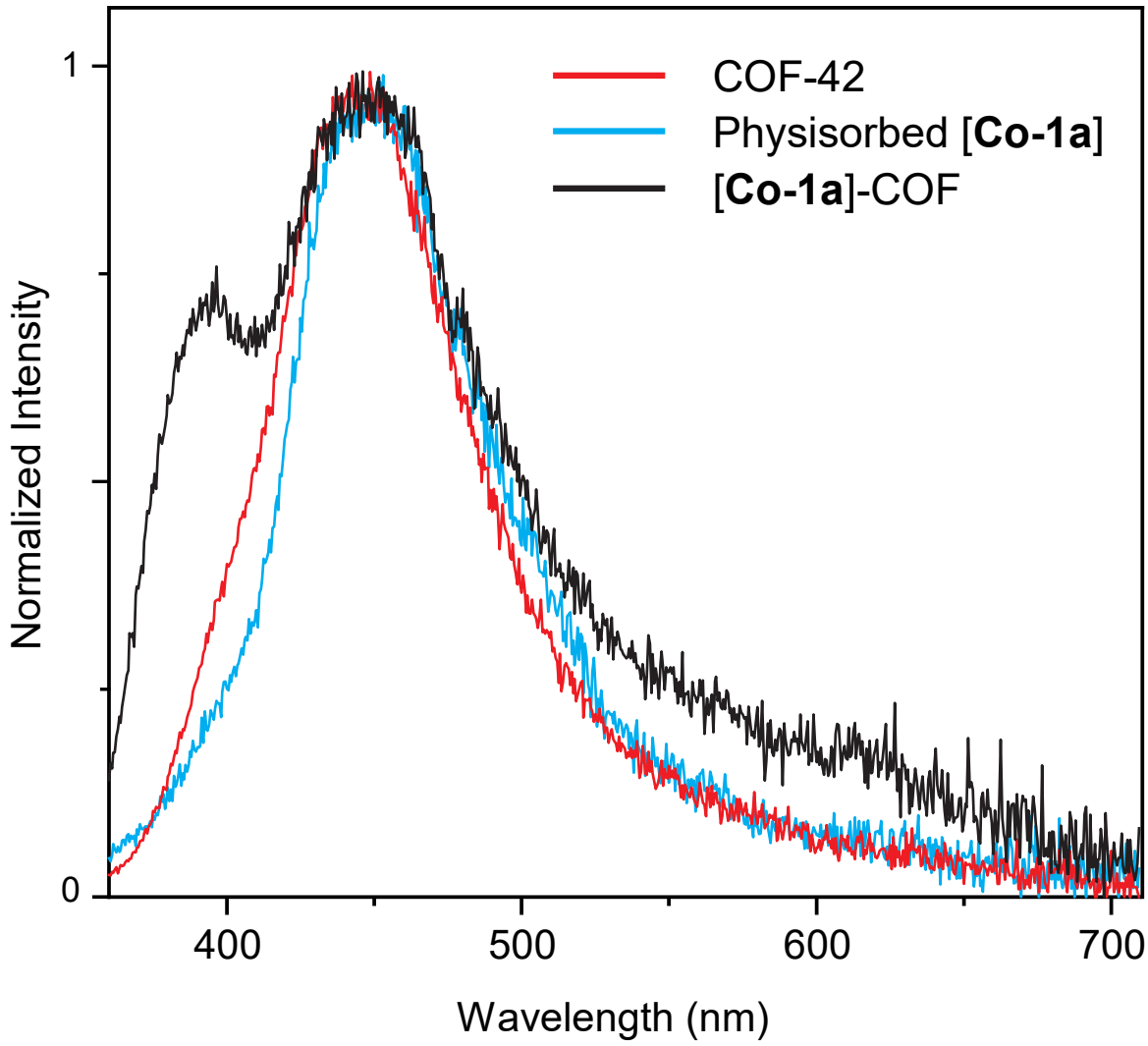

Figure S13: Emission spectra of COF-42, physisorbed [**Co-1a**], and [**Co-1a**]-COF. All samples were suspended in acetonitrile. All samples were excited at 300 nm.

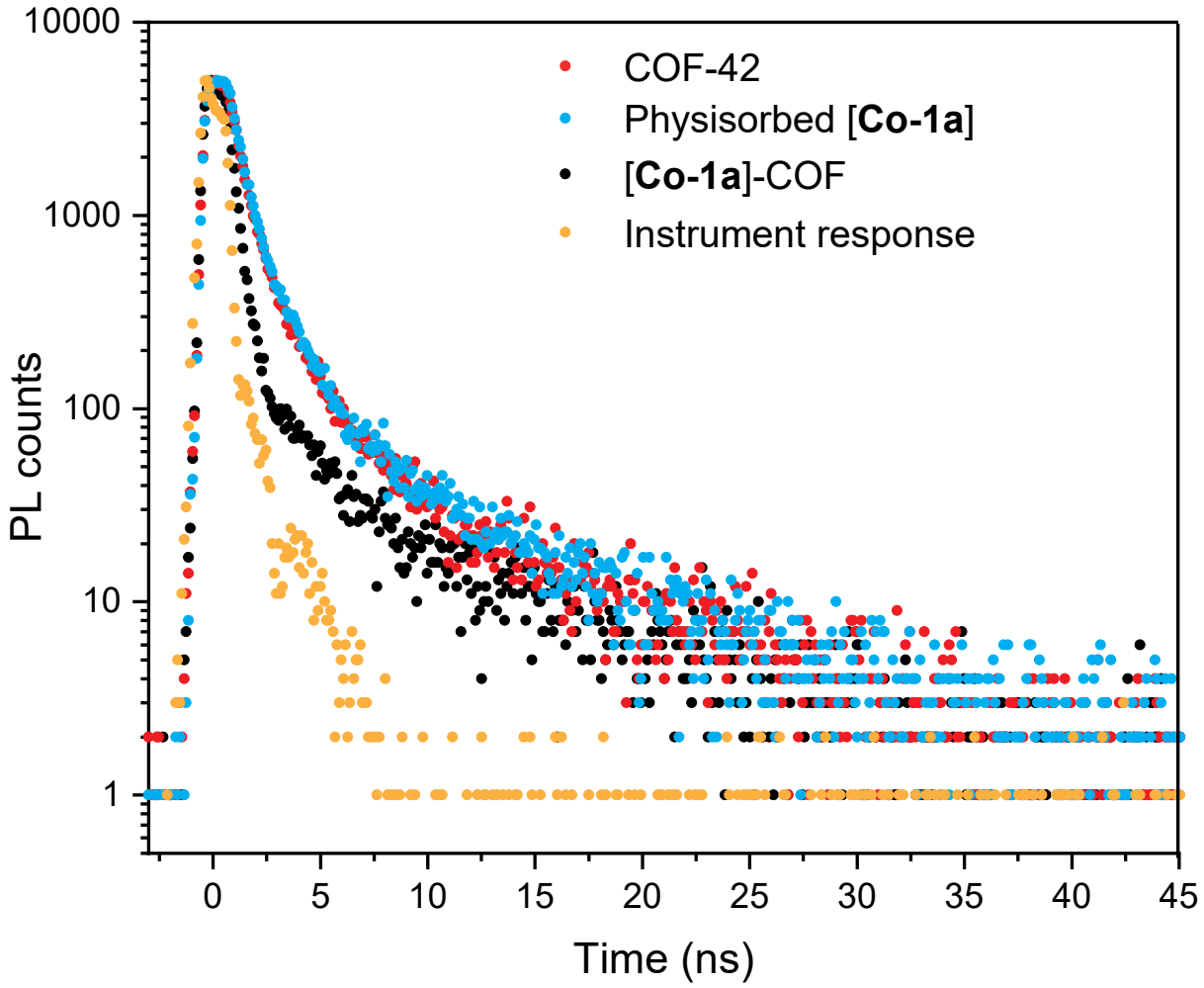

Figure S14: Fluorescence lifetime measurements of COF-42, physisorbed [**Co-1a**], and [**Co-1a**]-COF. All samples were suspended in acetonitrile. Samples were excited at 375 nm and the decay of the emission was monitored at 456 nm.

Emission spectra were recorded following excitation of [**Co-1a**]-COF, physisorbed [**Co-1a**] and only COF-42 samples at 300 nm. The poor dispersibility as well as the poorly emissive character of the samples prevented accurate measurement of absolute quantum yields ($< 1\%$) and relative emission intensities correctly and thus we present the normalized emission spectra of these three samples. We observe that while the emission spectra of physisorbed [**Co-1a**] and COF-42 only samples are identical, the spectrum for [**Co-1a**]-COF has two new emission features at 390 nm and around 550 – 600 nm. While we are presently uncertain about the origin of the former emission feature, we believe the latter emission feature could correspond

to charge transfer interaction between the COF backbone and the co-catalyst. We further attempted to evaluate the quenching of the photoexcited COF by cobaloxime using time correlated single photon counting (TCSPC) technique. The samples were excited using a 372 nm LASER source and the time decay of the emission was monitored at 456 nm. In comparison to physisorbed [**Co-1a**] sample, the emission decay for the covalently tethered [**Co-1a**]]-COF is observed to be faster. This faster decay could correspond to relaxation of the locally excited state to the charge transfer state in [**Co-1a**]-COF and hence better charge transfer due to close contact and confinement of the cobaloxime co-catalyst. The 310 ps component in the decay of [**Co-1a**]-COF possibly hints to the fast charge separation in the covalently linked sample and could be a possible contributing factor towards its improved photocatalytic activity. Unfortunately, attempts to monitor the lifetime of the emission at ca. 600 nm were hindered due to the extremely low emission counts at that wavelength thus preventing an analysis of the population of this possible charge transfer state and subsequent recombination kinetics.

Table S2: Emission lifetimes of COF-42, physisorbed [**Co-1a**] and [**Co-1a**]-COF.

Sample	Lifetime (weight factor)
COF-42	τ_1 = 0.48 ns (65.26%)
	τ_2 = 1.48 ns (26.76%)
	τ_3 = 7.63 ns (7.98%)
physisorbed [**Co-1a**]	τ_1 = 0.48 ns (63.56%)
	τ_2 = 1.48 ns (28.12%)
	τ_3 = 7.63 ns (8.32%)
[**Co-1a**]-COF	τ_1 = 0.31 ns (93.19%)
	τ_2 = 6.46 ns (6.81%)

ICP analysis

Table S3: Calculated catalyst content in weight percent according to ICP measurements. Functionalization of total amount of propargyl units in the $pCOF_{10}$ sample.

Sample name	Catalyst content (wt%)	Functionalization degree (%)
[**Co-1a**]-COF Route I	4.1	16
[**Co-1a**]-COF Route II	1.2	4.9
[**Co-1b**]-COF Route I	1.2	4.9
[**Co-1b**]-COF Route I	3.2	13
[**Co-1b**]-COF Route I	3.8	15
[**Co-1b**]-COF Route II	2.4	9.5
[**Co-2**]-COF Route I	3.5	15
[**Co-2**]-COF Route II	0.47	2.0

FTIR spectra

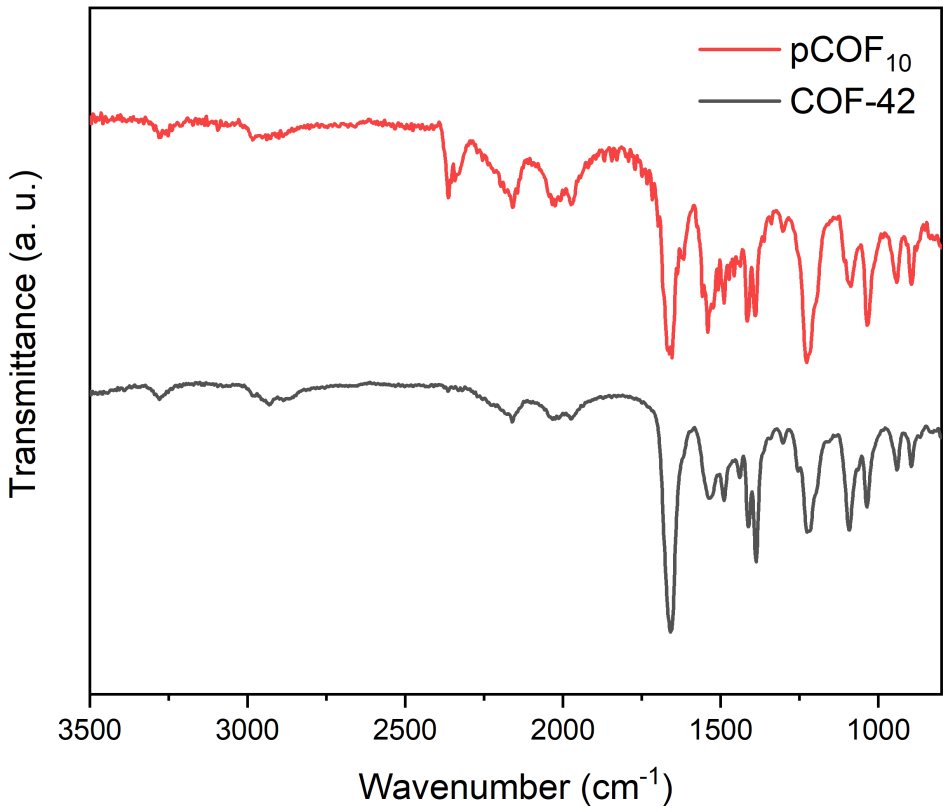

Figure S15: FTIR spectra of COF-42 and $pCOF_{10}$.

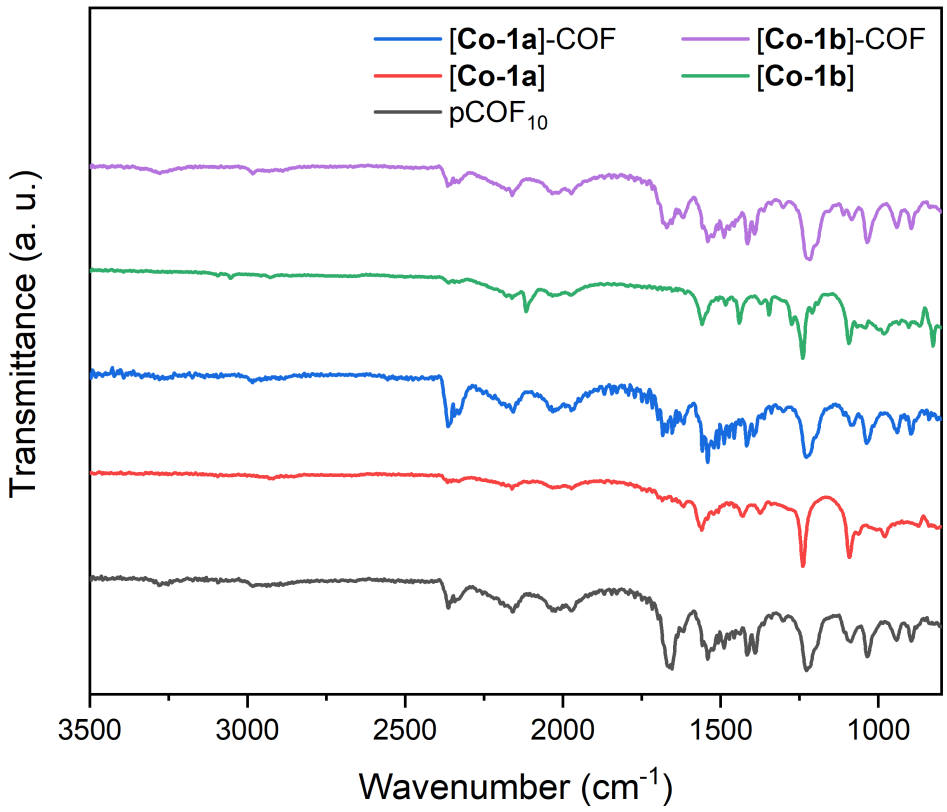

Figure S16: FTIR spectra of $pCOF_{10}$, [**Co-1a**], [**Co-1a**]-COF, [**Co-1b**], and [**Co-1b**]-COF.

UV/Vis absorption spectra

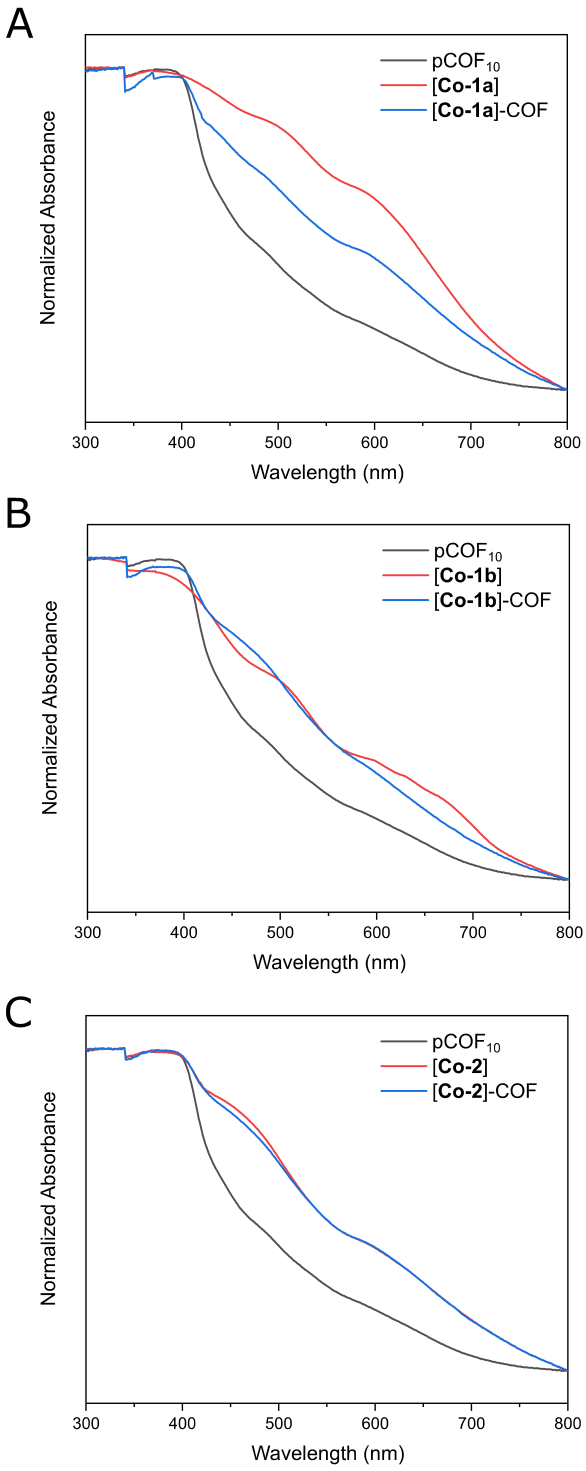

Figure S17: UV/Vis absorption spectra of (A) $pCOF_{10}$, [**Co-1a**] and [**Co-1a**]-COF; (B) $pCOF_{10}$, [**Co-1b**] and [**Co-1b**]-COF; (C) $pCOF_{10}$, [**Co-2**] and [**Co-2**]-COF.

Additional NMR measurements

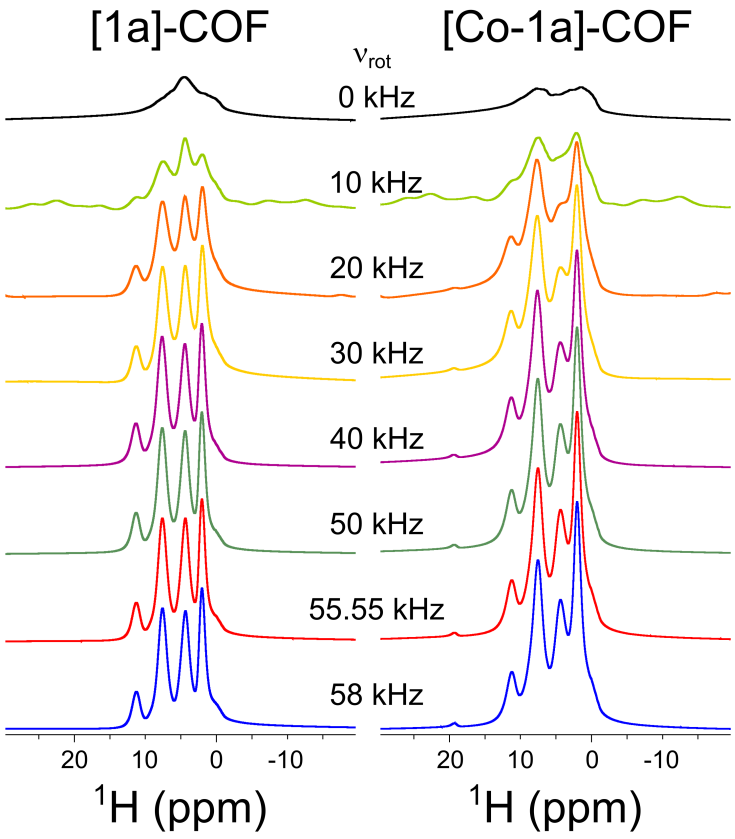

Figure S18: Dependence of the ^{1}H 1D spectrum quality of [**1a**]-COF and [**Co-1a**]-COF on the applied MAS frequency.

Quantum-Chemical Calculations

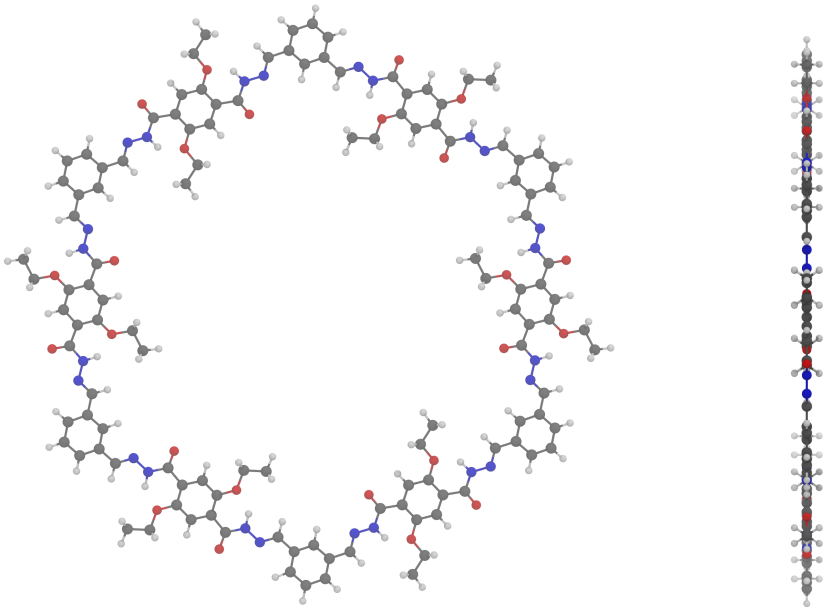

Figure S19: Optimized geometry for the COF-42 pore model, obtained on RI-PBE-D3/def2-TZVP level of theory. Top and side view.

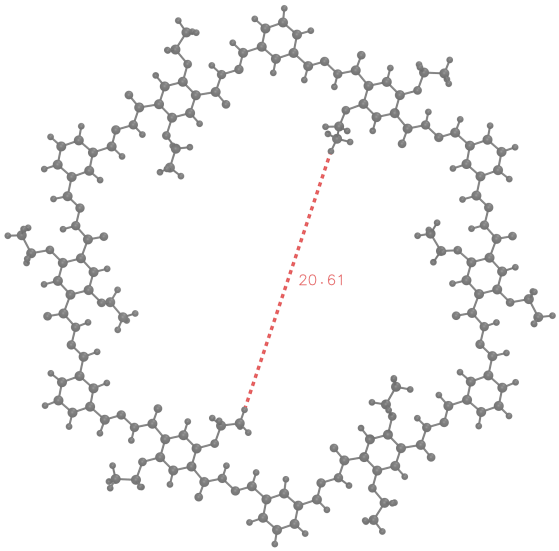

Figure S20: Visualization of the calculated pore diameter of 20.61 Åobtained from the optimized COF-42 pore model.

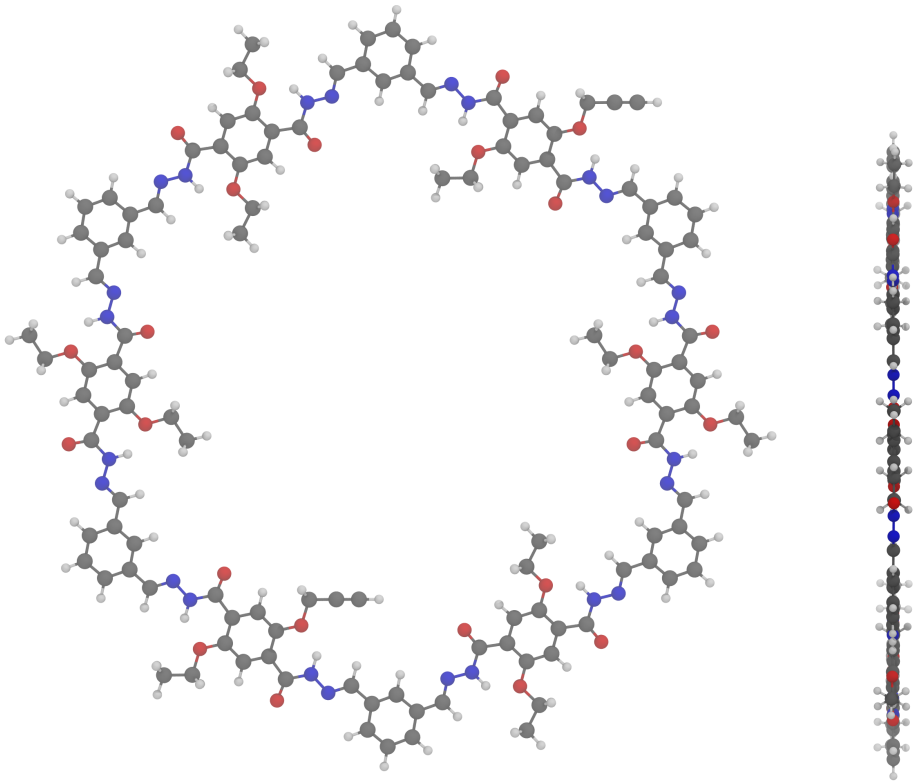

Figure S21: Optimized $pCOF_{10}$ pore model, obtained on RI-PBE-D3/def2-TZVP level of theory. Top and side view.

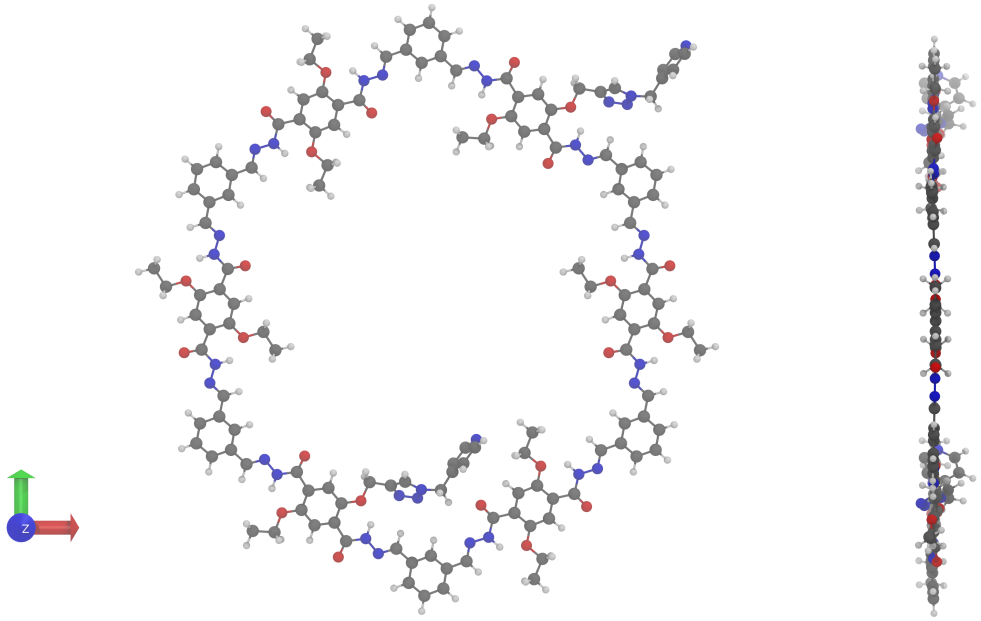

Figure S22: Optimized COF-42-pPy pore, obtained on RI-PBE-D3/def2-TZVP level of theory. Top and side view.

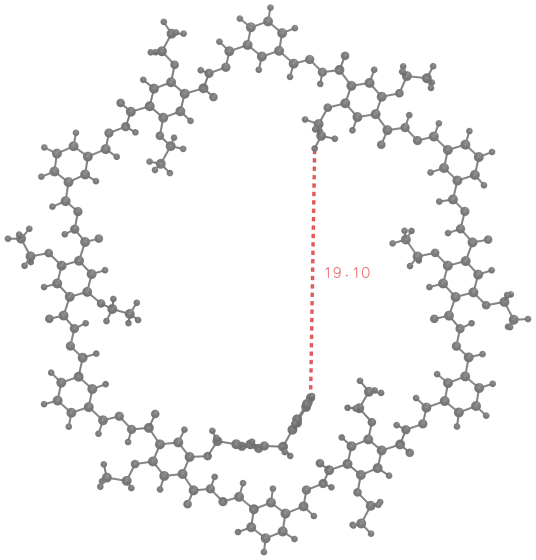

Figure S23: Visualization of the calculated pore diameter of 19.10 Åfor the COF42-pPy-COF pore model.

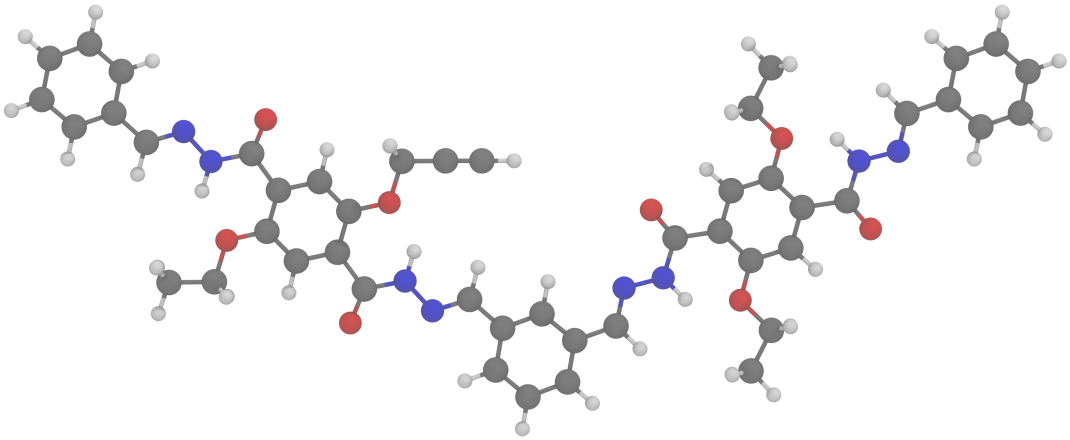

Figure S24: Geometry for the $pCOF_{10}$ cut model system, obtained by cutting the optimized $pCOF_{10}$ pore model.

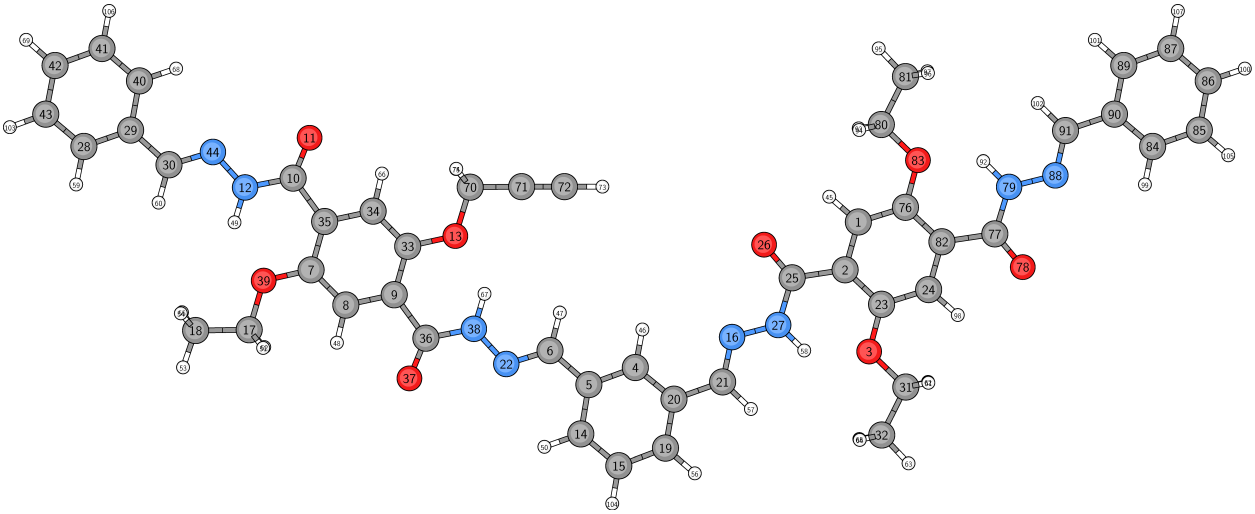

Figure S25: Atom labels for the $pCOF_{10}$ cut model system.

Table S4: Calculated NMR Chemical Shifts for the $pCOF_{10}$ model system, obtained on B97-2/pcS-2//RI-PBE-D3/def2-TZVP level of theory.

Atom Number	Element	NMR Chemical Shielding [ppm]	NMR Chemical Shift [ppm]
1	C	61.75	123.39
2	C	53.85	131.29
3	O	198.64	-
4	C	49.14	136.00
5	C	40.88	144.25
6	C	32.21	152.92
7	C	24.56	160.57
8	C	61.25	123.89
9	C	53.21	131.93
10	C	17.82	167.32
11	O	-76.77	-
12	N	50.70	-211.18
13	O	209.02	-
14	C	48.12	137.02
15	C	46.87	138.27
16	N	-99.68	-60.80
17	C	113.68	71.46
18	C	167.00	18.14
19	C	46.29	138.85
20	C	42.21	142.92
21	C	34.25	150.89
22	N	-102.74	-57.74
23	C	24.97	160.17

Continued on the next page...

Table S4: Continued: Calculated NMR Chemical Shifts for the $pCOF_{10}$ model system, obtained on B97-2/pcS-2//RI-PBE-D3/def2-TZVP level of theory.

Atom Number	Element	NMR Chemical Shielding [ppm]	NMR Chemical Shift [ppm]
24	C	61.42	123.71
25	C	17.25	167.89
26	O	-73.41	-
27	N	50.91	-211.39
28	C	46.61	138.52
29	C	42.36	142.78
30	C	33.51	151.63
31	C	113.79	71.34
32	C	167.04	18.09
33	C	26.28	158.85
34	C	62.74	122.39
35	C	53.62	131.52
36	C	18.13	167.01
37	O	-75.58	-
38	N	50.09	-210.57
39	O	198.26	-
40	C	49.19	135.94
41	C	46.70	138.43
42	C	46.31	138.83
43	C	48.57	136.56
44	N	-100.95	-59.53
45	H	22.82	8.57
46	H	22.63	8.75

Continued on the next page...

Table S4: Continued: Calculated NMR Chemical Shifts for the $pCOF_{10}$ model system, obtained on B97-2/pcS-2//RI-PBE-D3/def2-TZVP level of theory.

Atom Number	Element	NMR Chemical Shielding [ppm]	NMR Chemical Shift [ppm]
47	H	22.99	8.40
48	H	22.76	8.63
49	H	19.32	12.07
50	H	22.56	8.83
51	H	27.03	4.36
52	H	27.05	4.34
53	H	29.83	1.56
54	H	29.59	1.80
55	H	29.59	1.80
56	H	24.00	7.39
57	H	23.32	8.07
58	H	19.25	12.14
59	H	23.95	7.44
60	H	23.34	8.05
61	H	27.05	4.34
62	H	27.04	4.35
63	H	29.83	1.55
64	H	29.57	1.82
65	H	29.57	1.82
66	H	23.01	8.38
67	H	19.14	12.24
68	H	22.46	8.93
69	H	23.79	7.60

Continued on the next page...

Table S4: Continued: Calculated NMR Chemical Shifts for the $pCOF_{10}$ model system, obtained on B97-2/pcS-2//RI-PBE-D3/def2-TZVP level of theory.

Atom Number	Element	NMR Chemical Shielding [ppm]	NMR Chemical Shift [ppm]
70	C	122.65	62.49
71	C	104.10	81.03
72	C	100.32	84.82
73	H	28.40	2.99
74	H	26.36	5.02
75	H	26.39	5.00
76	C	24.98	160.15
77	C	17.55	167.58
78	O	-79.09	-
79	N	51.03	-211.50
80	C	113.81	71.32
81	C	166.98	18.16
82	C	53.48	131.66
83	O	199.13	-
84	C	49.11	136.02
85	C	46.72	138.41
86	C	46.00	139.14
87	C	48.51	136.63
88	N	-101.30	-59.18
89	C	47.25	137.88
90	C	42.32	142.81
91	C	34.27	150.86
92	H	19.37	12.02

Continued on the next page...

Table S4: Continued: Calculated NMR Chemical Shifts for the $pCOF_{10}$ model system, obtained on B97-2/pcS-2//RI-PBE-D3/def2-TZVP level of theory.

Atom Number	Element	NMR Chemical Shielding [ppm]	NMR Chemical Shift [ppm]
93	H	27.02	4.37
94	H	27.04	4.35
95	H	29.77	1.62
96	H	29.58	1.81
97	H	29.58	1.81
98	H	22.80	8.59
99	H	22.44	8.95
100	H	23.78	7.61
101	H	23.95	7.44
102	H	23.34	8.04
103	H	23.87	7.52
104	H	23.76	7.63
105	H	23.73	7.66
106	H	23.71	7.68
107	H	23.86	7.53

End of Table S4

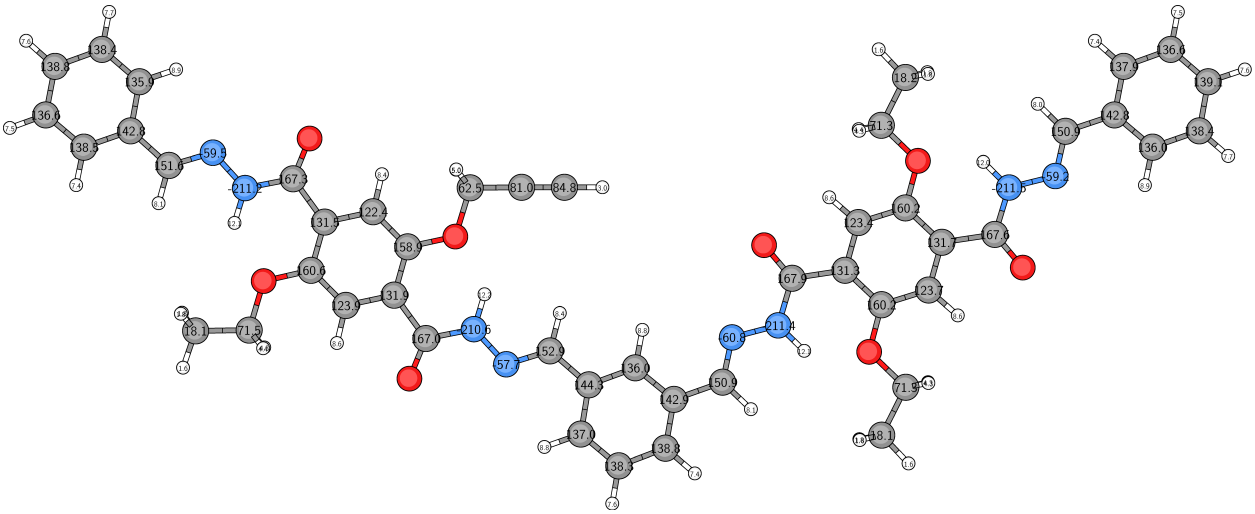

Figure S26: Calculated NMR Chemical Shifts for the $pCOF_{10}$ cut model system, obtained on B97-2/pcS-2//RI-PBE-D3/def2-TZVP level of theory.

Molecular Dynamics Simulations

14970 equidistant frames of a [**1a**]-COF pore consisting of 155 atoms were extracted from a 15 ns molecular dynamic simulation. To avoid bending, twisting and major distortion of the backbone, which is unlikely to happen in an extended, π-π-stacked 2D material, the atomic coordinates of all non-hydrogen backbone atoms were constrained in plane, whereas atoms of the ethoxy groups and the entire **1a** ligand were allowed to move. The high mobility of the **1a** ligand is reflected in the plethora of the positions that the ligand can occupy (Figure S28). It was seen that the hydrogen bond between the nitrogen atoms of the triazol ring and the NH backbone proton is not strong enough to hinder the rotation of the **1a** group along the rotatable bond between C13 and C14. Fig. S28 displays all coordinates that the para-nitrogen atom of the pyridine group visited during the simulation. In the bulk material, the stacking of the 2D layers on the top of each other would hinder the **1a** group to move into the periphery of the pore, thus all frames where the **1a** linker moved more than ± 2 Å out of the COF plane were discarded, leaving 3730 frames. The complexation of the covalent ligand with the cobaloxime group is expected to reduce the mobility of **Co-1a** even further due to steric hindrance. To narrow down possible conformations that [**Co-1a**]-COF can occupy, the cobaloxime molecule was docked to the pyridine group to all remaining frames. Since the cobaloxime can freely rotate around the axis defined by the pyridine N-Co-Cl axis, the Cobaloxime orientation was sampled by rotating it in 18 ten-degree steps. Structures with close contacts between the cobaloxime and the pore wall atoms were rejected resulting in a total of 60321 possible structures. In order to investigate a representative set of models, 200 structures with the largest possible structural diversity were selected, cut to the size of the cut model system to then calculate NMR chemical shifts on B97-2/pcSseg-1[15,16] level of theory using the FermiONs++[17,18] program package.

Calculated NMR chemical shifts together with the corresponding structures were then used to simulate 2D ^{1}H-^{1}H DQ-SQ as well as 2D ^{1}H-^{13}C correlation spectra. For the simulation

of the DQ-SQ spectra, only those ^{1}H-^{1}H pairs were taken into consideration which were maximum 3.5 Å away from each other. The signal intensity of each peak was scaled by r^{-3} (ref. 20), and the corresponding peaks were artificially broadened assuming a Gaussian line shape with 0.5 ppm line-broadening in both dimensions. For the ^{1}H-^{13}C spectrum simulations, both 6 and 2 Å distance cutoffs were used, replicating the experimental 500 and 2250 μs CP transfer conditions, and signal intensities were scaled with a r^{-2} function which partially accounts for the relayed magnetization transfer at distant sites due to spin diffusion. Lines were then broadened by 0.5 and 2.0 ppm in the ^{1}H and ^{13}C dimensions, respectively. To further facilitate the direct comparison of the simulated and measured spectra, signal intensities were scaled according to their expected abundance: As the experimental ^{1}H 1D spectrum of [**Co-1a**]-COF suggests a 2 n% functionalization degree, the simulated cross-peak intensities between the ligand and the backbone resonances were scaled down by a factor of 50.

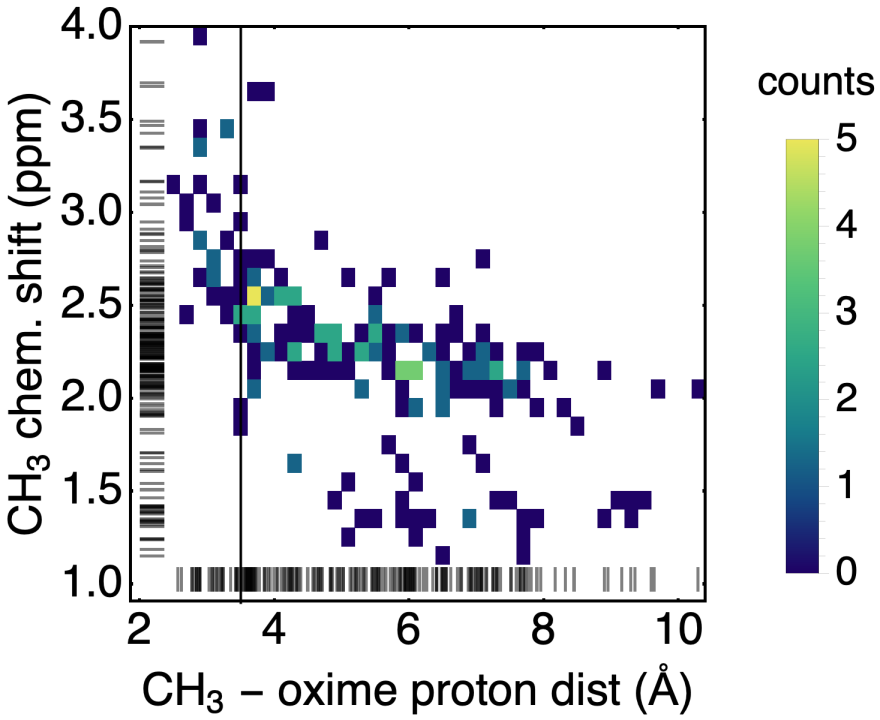

Figure S27: Distribution of the calculated methyl proton chemical shifts vs the distance between the methyl and oxime protons for 200 example MD frames calculated on B97-2/pcSseg-1[15,16] level of theory using the FermiONs++[17,18] program package. Solid vertical line marks the 3.5 Å limit below which the DQ-SQ peak is expected the appear in the NMR spectra.

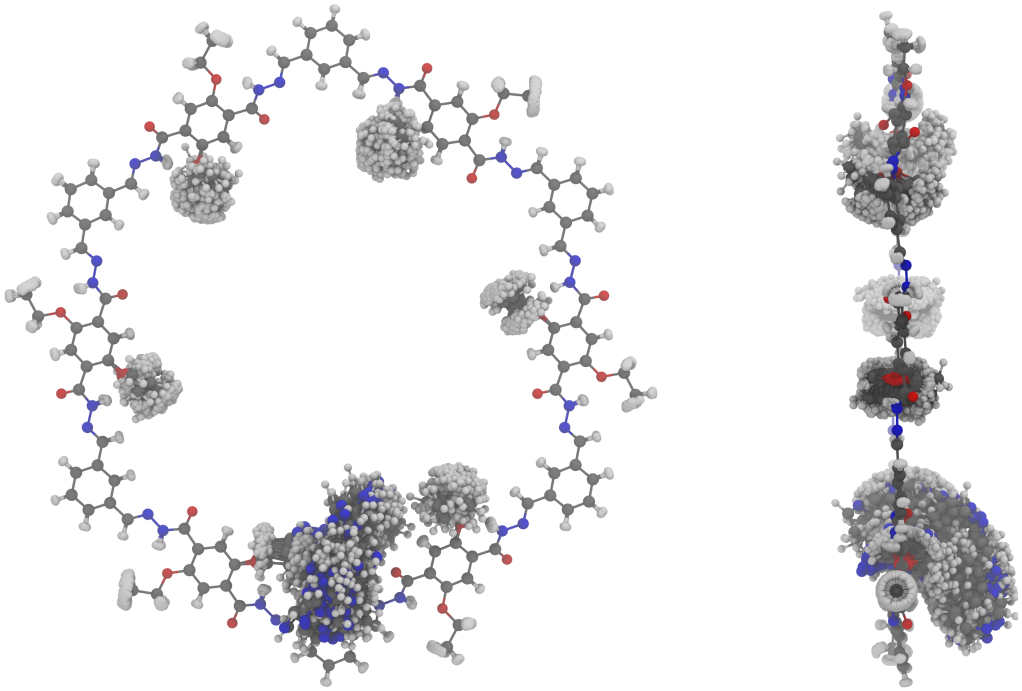

Figure S28: Overlay of every 100th frame from a 15 ns MD simulation visualizing the flexibility of the **1a**-ligand in comparison to the ethoxy-ligands. Top and side view.

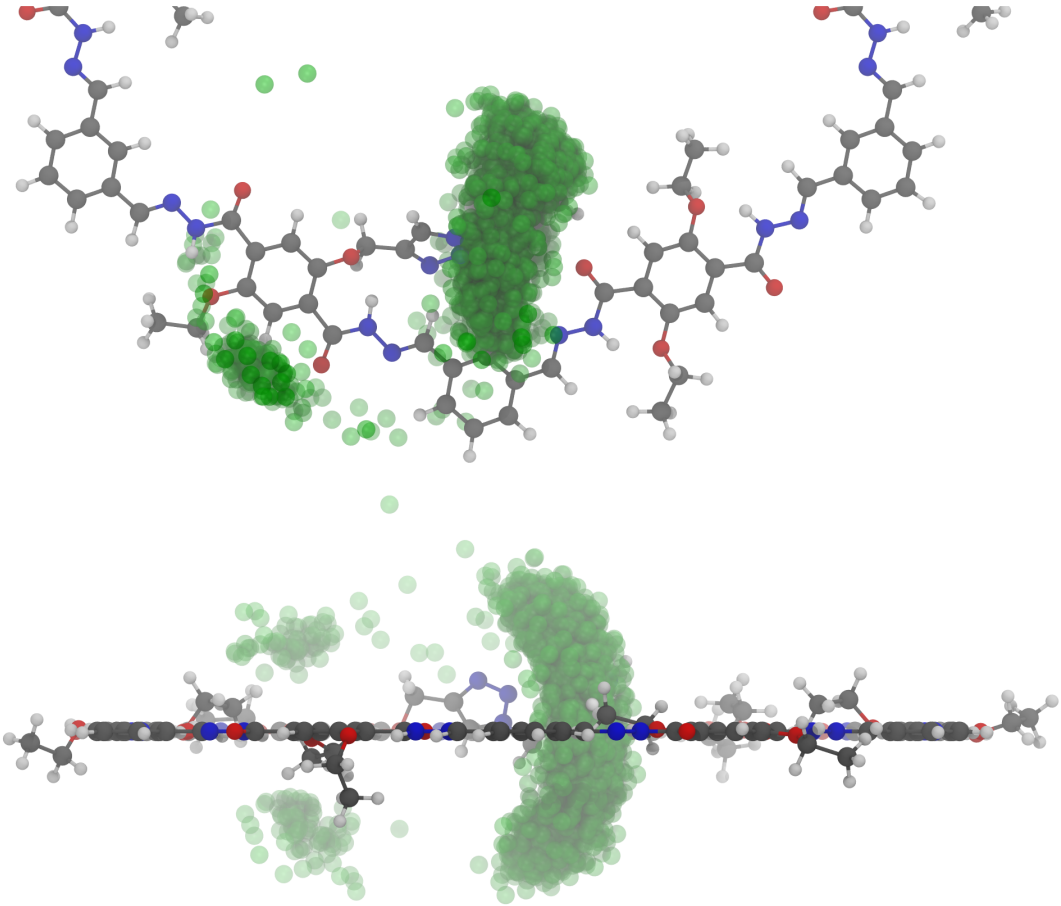

Figure S29: Overlay of every nitrogen position of the **1a**-ligand showing positions from every 5th frame from a 15 ns MD simulation visualizing visited positions of the Pyridine subunit. Top and side view.

References

(1) Perdew, J. P.; Burke, K.; Ernzerhof, M. Generalized Gradient Approximation Made Simple. *Physical Review Letters* **1996**, *77*, 3865–3868.

(2) Grimme, S.; Antony, J.; Ehrlich, S.; Krieg, H. A consistent and accurate ab initio parametrization of density functional dispersion correction (DFT-D) for the 94 elements H-Pu. *The Journal of Chemical Physics* **2010**, *132*, 154104.

(3) Schäfer, A.; Huber, C.; Ahlrichs, R. Fully optimized contracted Gaussian basis sets of triple zeta valence quality for atoms Li to Kr. *The Journal of Chemical Physics* **1994**, *100*, 5829–5835.

(4) Eichkorn, K.; Weigend, F.; Treutler, O.; Ahlrichs, R. Auxiliary basis sets for main row atoms and transition metals and their use to approximate Coulomb potentials. *Theoretical Chemistry Accounts: Theory, Computation, and Modeling (Theoretica Chimica Acta)* **1997**, *97*, 119–124.

(5) Burow, A. M.; Sierka, M.; Mohamed, F. Resolution of identity approximation for the Coulomb term in molecular and periodic systems. *The Journal of Chemical Physics* **2009**, *131*, 214101.

(6) Grajciar, L. Low-memory iterative density fitting. *Journal of Computational Chemistry* **2015**, *36*, 1521–1535.

(7) Burow, A. M.; Sierka, M. Linear Scaling Hierarchical Integration Scheme for the Exchange-Correlation Term in Molecular and Periodic Systems. *Journal of Chemical Theory and Computation* **2011**, *7*, 3097–3104.

(8) Łazarski, R.; Burow, A. M.; Sierka, M. Density Functional Theory for Molecular and Periodic Systems Using Density Fitting and Continuous Fast Multipole Methods. *Journal of Chemical Theory and Computation* **2015**, *11*, 3029–3041.

(9) Łazarski, R.; Burow, A. M.; Grajciar, L.; Sierka, M. Density functional theory for molecular and periodic systems using density fitting and continuous fast multipole method: Analytical gradients. *Journal of Computational Chemistry* **2016**, *37*, 2518–2526.

(10) TURBOMOLE (V7.1 2016). University of Karlsruhe and Forschungszentrum Karlsruhe GmbH, 1989-2007, TURBOMOLE GmbH, since 2007. Available at http://www.turbomole.com.

(11) Wang, J.; Wang, W.; Kollman, P. A.; Case, D. A. Automatic atom type and bond type perception in molecular mechanical calculations. *Journal of Molecular Graphics and Modelling* **2006**, *25*, 247–260.

(12) Phillips, J. C.; Braun, R.; Wang, W.; Gumbart, J.; Tajkhorshid, E.; Villa, E.; Chipot, C.; Skeel, R. D.; Kalé, L.; Schulten, K. Scalable molecular dynamics with NAMD. *Journal of Computational Chemistry* **2005**, *26*, 1781–1802.

(13) D.A. Case, R.M. Betz, D.S. Cerutti, T.E. Cheatham, III, T.A. Darden, R.E. Duke, T.J. Giese, H. Gohlke, A.W. Goetz, N. Homeyer, S. Izadi, P. Janowski, J. Kaus, A. Kovalenko, T.S. Lee, S. LeGrand, P. Li, C. Lin, T. Luchko, R. Luo, B. Madej, D. Mermelstein, K.M. Merz, G. Monard, H. Nguyen, H.T. Nguyen, I. Omelyan, A. Onufriev, D.R. Roe, A. Roitberg, C. Sagui, C.L. Simmerling, W.M. Botello-Smith, J. Swails, R.C. Walker, J. Wang, R.M. Wolf, X. Wu, L. Xiao and P.A. Kollman (2016), AMBER 2016, University of California, San Francisco.

(14) Wang, J.; Wolf, R. M.; Caldwell, J. W.; Kollman, P. A.; Case, D. A. Development and testing of a general amber force field. *Journal of Computational Chemistry* **2004**, *25*, 1157–1174.

(15) Wilson, P. J.; Bradley, T. J.; Tozer, D. J. Hybrid exchange-correlation functional de-

termined from thermochemical data and ab initio potentials. *The Journal of Chemical Physics* **2001**, *115*, 9233–9242.

(16) Jensen, F. Segmented Contracted Basis Sets Optimized for Nuclear Magnetic Shielding. *Journal of Chemical Theory and Computation* **2014**, *11*, 132–138.

(17) Kussmann, J.; Ochsenfeld, C. Preselective Screening for Linear-Scaling Exact Exchange-Gradient Calculations for Graphics Processing Units and General Strong-Scaling Massively Parallel Calculations. *Journal of Chemical Theory and Computation* **2015**, *11*, 918–922.

(18) Kussmann, J.; Ochsenfeld, C. Pre-selective screening for matrix elements in linear-scaling exact exchange calculations. *The Journal of Chemical Physics* **2013**, *138*, 134114.

(19) Kisch, H.; Bahnemann, D. Best Practice in Photocatalysis: Comparing Rates or Apparent Quantum Yields? *The Journal of Physical Chemistry Letters* **2015**, *6*, 1907–1910.

(20) Pileio, G.; Concistrè, M.; McLean, N.; Gansmüller, A.; Brown, R. C.; Levitt, M. H. Analytical theory of γ-encoded double-quantum recoupling sequences in solid-state nuclear magnetic resonance. *Journal of Magnetic Resonance* **2007**, *186*, 65–74.